Aus dem

Department für Diagnostische Labormedizin der Universität Tübingen

Institut für Medizinische Mikrobiologie und Hygiene

Sektion für Zelluläre und Molekulare Mikrobiologie

Exploring the Role of the SctW-SctV Interaction in Substrate Specificity Switching of Salmonella's Type III Secretion System-1

Inaugural-Dissertation
zur Erlangung des Doktorgrades
der Medizin

der Medizinischen Fakultät
der Eberhard Karls Universität
zu Tübingen

vorgelegt von

Schönwald, Clara Maria

2025

Dekan:	Professor Dr. B. Pichler
1. Berichterstatter:	Professor Dr. S. Wagner
2. Berichterstatter:	Privatdozentin Dr. M. Schütz
3. Berichterstatter:	Professor Dr. M. Schindler

Tag der Disputation: 13.12.2024

Table of contents

Abbreviations

Å	Ångström
ACA	aminocaproic acid
Amp	ampicillin
ATP	adenosine triphosphate
ATPase	adenosine triphosphatase
BN	Blue Native
bp	base pairs
cm	crude membranes
Cm	chloramphenicol
DAP	diaminopimelic acid
DNA	deoxyribonucleic acid
dNTP	deoxynucleosid triphosphate
DTT	dithiothreitol
E. coli	*Escherichia coli*
e.g.	for example
EDTA	ethylendiaminetetraacetate
et al.	and others
Kan	kanamycin
kDa / MDa	kilodalton / megadalton
LB	lysogeny broth
LMNG	lauryl maltose neopentyl glycol
NAD	β-nicotinamide adenine dinucleotide
NL	NanoLuc luciferase
o/n	overnight
OD_{600}	optical density for the wavelength of 600 nm
ODU	optical density (per millilitre)
PAGE	polyacrylamide gel electrophoresis
***p*Bpa**	*para*-benzoyl-L-phenylalanine
PBS	phosphate-buffered saline
PCR	polymerase chain reaction
PEG	polyethylene glycol

pT10	pTACO10 (from: *T*ight *A*nd *CO*ntrolled)
PVDF	polyvinylidene difluoride
QC	QuikChange site-directed mutagenesis
rpm	revolutions per minute
RT	room temperature
***S.* Typhimurium**	*Salmonella* Typhimurium
Sct	secretion and cellular translocation
SD	subdomain
SDS	sodium dodecyl sulfate
sn	supernatant
SOB	super optimal broth
SOC	super optimal broth with catabolite repression
SPI-1	*Salmonella* pathogenicity island 1
SPI-2	*Salmonella* pathogenicity island 2
Strep	streptomycin
T3SS	type III secretion system
TAE	Tris-acetate buffer with EDTA
Taq	*Thermus aquaticus*
TBS	Tris-buffered saline
TBS-T	Tris-buffered saline with Tween 20
TCA	trichloroacetic acid
Tet	tetracycline
TEV	tobacco etch virus
TMD	transmembrane domain
Tris	tris(hydroxymethyl)aminomethane
tRNA	transfer ribonucleic acid
UV	ultraviolet
w/v	weight per volume
wc	whole cells
wt	wild type

List of figures and tables

1.1 Tables

1.2 Figures

2 Introduction

Salmonella enterica subspecies *enterica* serovar Typhimurium (*S*. Typhimurium) is a rod-shaped, gram-negative bacterium, that poses a serious public health threat (Ehuwa, Jaiswal and Jaiswal, 2021). It leads to infection after ingestion of contaminated water and food, such as meat and fish (Heinitz et al., 2000; Meyer et al., 2010). *S.* Typhimurium is responsible for an estimated 100 million cases of nontyphoidal *Salmonella* gastroenteritis annually (Majowicz *et al.*, 2010). While most cases of salmonellosis are self-limiting and can be treated symptomatically, vulnerable populations, such as children and the elderly, are at the risk of severe dehydration that can be life-threatening (WHO, 2018). As a result, non-typhoidal *Salmonella* enterica ranks as the third leading cause of death among food-borne diseases worldwide (WHO, 2015). The increasing prevalence of antibiotic resistance further complicates treatment and biocontrol efforts (Cui *et al.*, 2008; Patra *et al.*, 2021).

To address these challenges, a deeper understanding of the molecular processes underlying bacterial pathogenicity is essential. A key aspect of pathogenicity involves the role of virulence factors, which enable effective infection of host cells. Studying these factors not only provides insights into the mechanisms of infectious diseases and bacterial evolution but also contributes to the development of novel therapeutic strategies (McShan and de Guzman, 2015). This introduction will provide an overview of the type III secretion system (T3SS) employed by *S.* Typhimurium, focusing on the gatekeeper protein InvE and its role in the regulation of virulence factors secretion.

2.1 Bacterial pathogenicity and secretion

Successful bacterial infection depends on the proximity of a pathogen to its host and the ability to overcome host defenses, such as the immune response, by intentionally altering the microenvironment (Teitzel, 2013). Pathogenicity factors facilitate the infection of the host by mediating bacterial entry, promoting cellular

adherence, and ensuring the pathogens' survival within the host, ultimately leading to infection (Gal-Mor and Finlay, 2006). These factors also play a crucial role in determining the virulence of *S.* Typhimurium (Fatica and Schneider, 2011).

Secretion systems serve as essential pathogenicity factors and are widespread among many clinically relevant pathogens. Among them, gram-negative bacteria, with their complex cell envelope, utilize these intricate multi-protein nanomachines to transfer virulence effector proteins into their target cells. Recent advances in research have identified eleven secretion systems in gram-negative bacteria to date (Grossman *et al.*, 2021). These systems serve various biological purposes, including nutrient acquisition, biofilm formation, and host cell invasion. While sharing some basic characteristics, each system possesses distinct architectures, mechanisms of secretion, and energy dependencies tailored to their specific organism and function (Costa *et al.*, 2015a; Galán and Waksman, 2018; Grossman *et al.*, 2021).

2.2 Type III Secretion Systems in *Salmonella* Typhimurium

Salmonella Typhimurium employs type III secretion systems (T3SS) for host cell invasion and infection. T3SS, also known as injectisomes, are conserved across many gram-negative bacteria, including Enteropathogenic / Enterohemorrhagic *Escherichia coli* (EPEC/EHEC), *Pseudomonas aeruginosa, Salmonella*, *Shigella* and *Yersinia* species (Galán *et al.*, 2014; Costa *et al.*, 2015b). These double-membrane-spanning needle-like molecular machines are one of the most sophisticated and well-studied secretion systems, playing a key factor to the virulence of many enteric pathogens (dos Santos, Ferrari and Conte-Junior, 2020). They consist of approximately 25 different protein subunits, each with varying copy numbers (Zilkenat *et al.*, 2016).

A.

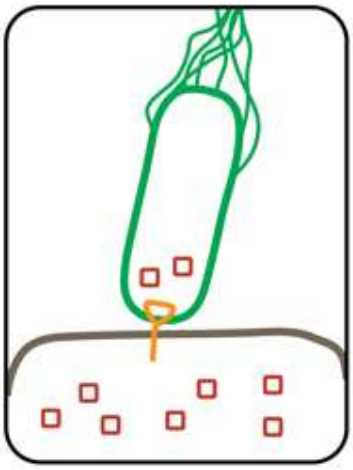

B.

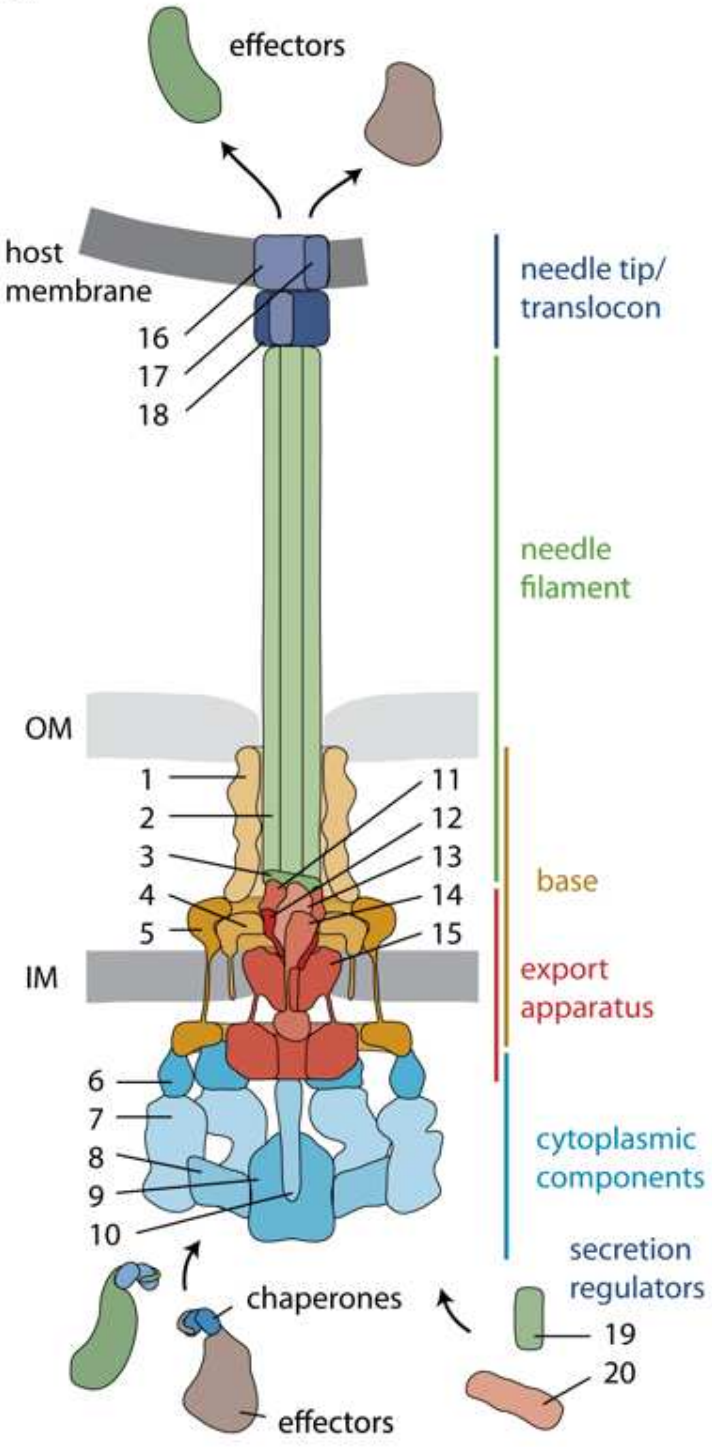

C.

#	Uni	SPI-1
1	SctC	InvG
2	SctF	PrgI
3	SctI	PrgJ
4	SctJ	PrgK
5	SctD	PrgH
6	SctK	OrgA
7	SctQ	SpaO
8	SctL	OrgB
9	SctN	InvC
10	SctO	InvI
11	SctR	SpaP
12	SctS	SpaQ
13	SctT	SpaR
14	SctU	SpaS
15	SctV	InvA
16	SctE	SipB
17	SctB	SipC
18	SctA	SipD
19	SctP	InvJ
20	SctW	InvE

Figure 1 **Schematic overview of the individual components of the fully assembled T3SS. A** Bacteria utilized T3SS to inject effector proteins into eukaryotic host cells. **B** Structure of the T3SS with structural subunits. OM: outer membrane, IM: inner membrane. **C** Unified nomenclature of T3SS components and SPI-1 homologs. (Modified after Wagner et al., 2018)

Since the first visualization of the *S.* Typhimurium T3SS using electron microscopy by Kubori et al., 1998, significant progress has been made in understanding the intricate composition of the needle complex (Kuhlen *et al.*, 2018). The injectisome can be subdivided into five subcomponents that contribute to the overall function of the type III secretion system: the base, the export apparatus, and the needle filament (collectively referred to as the needle complex), the translocon, and cytoplasmic components (see Figure 1). These subcomponents are classified based on their structural organization within the T3SS rather than their specific functions, which serves to improve our understanding of the system as a whole (reviewed in Wagner et al., 2018).

Because many subunit proteins are conserved across bacterial species in both function and structure, a unified *s*ecretion and *c*ellular *t*ranslocation (*Sct*) nomenclature was first proposed in 1998, and later extended (Hueck, 1998; Wagner and Diepold, 2020). In this project, the Sct nomenclature as presented by Deng et al., 2017 will be used (see Table 1).

The function of the syringe-like T3SS largely relies on its ability to deliver effector proteins into host cells. Upon recognition of the target environment, T3SS inject effector proteins through a hollow needle-like filament directly into the target cells, translocating unfolded proteins across bacterial and host cell membranes (Akeda and Galán, 2005; Mota, Sorg and Cornelis, 2005; Costa *et al.*, 2015b). This process relies on both ATP and the proton motor force (Wilharm *et al.*, 2004; Akeda and Galán, 2005). The diverse effector proteins modify host cell physiology in various ways, such as altering the host cell's actin cytoskeleton or suppressing cell death (Tosi *et al.*, 2013).

Assembly of the different subunits into a multi-MDa membrane-spanning machine requires precise coordination and occurs in distinct sequential steps (Diepold and Wagner, 2014)

Table 1 **Functional names and unified secretion and cellular translocation (Sct) nomenclature** for T3SS core structural proteins and their flagellar homologs (modified from Deng et al., 2017)

Unified nomenclature	**Proposed function**	***Salmonella* spp.**		***Yersinia* spp.**	**EPEC and EHEC**	***Shigella* spp.**	***P. aeruginosa***	***Chlamydia* spp.**	**Flagellar apparatus**
		SPI-1	**SPI-2**						
BASE									
SctC	Secretin, outer membrane ring	InvG	SsaC	YscC	EscC	MxiD	PscC	CdsC	-
SctD	Inner membrane ring	PrgH	SsaD	YscD	EscD	MxiG	PscD	CdsD	FliG
SctJ	Inner membrane ring	PrgK	SsaJ	YscJ	EscJ	MxiJ	PscJ	CdsJ	FliF
EXPORT APPARATUS									
SctV	Export gate	InvA	SsaV	YscV	EscV	MxiA	PcrD	CdsV	FlhA
SctR	Inner membrane component	SpaP	SsaR	YscR	EscR	Spa24	PscR	CdsR	FliP
SctS	Inner membrane component	SpaQ	SsaS	YscS	EscS	Spa9	PscS	CdsC	FliQ
SctT	Inner membrane component	SpaR	SsaT	YscT	EscT	Spa29	PscT	CdsT	FliR
SctU	Autoprotease	SpaS	SsaU	YscU	EscU	Spa40	PscU	CdsU	FlhB
NEEDLE FILAMENT									
SctF	Needle	PrgI	SsaG	YscF	EscF	MxiH	PscF	CdsF	FlgE
SctI	Needle adapter	PrgJ	SsaI	YscI	EscI	MxiI	PscI	-	-
TRANSLOCON									
SctB	Translocation pore	SipC	SseD	YopD	EspB	IpaC	PopD	CopD	-
SctE	Translocation pore	SipB	SseC	YopB	EspD	IpaB	PopB	CopB	-
SctA	Needle tip or filament	SipD	SseB	LcrV	EspA	IpaD	PcrV	CT584	FliC
CYTOPLASMIC COMPONENTS									
SctQ	Cytoplasmic ring	SpaO	SsaQ	YscQ	SepQ	Spa33	PscQ	CdsQ	FliM-FliN
SctN	ATPase	InvE	SsaN	YscN	EscN	Spa47	PscN	CdsC	FliI
SctL	Stator	OrgB	SsaK	YscL	EscL	MxiN	PscL	CdsL	FliH
SctO	Stalk	InvI	SsaO	YscO	EscO	Spa13	PscO	CdsO	FliJ
SctK	ATPase cofactor	OrgA	-	YscK	EscK	MxiK	PscK	-	-
REGULATORS									
SctP	Needle-length regulator	InvJ	SsaP	YscP	EscP	Spa32	PscP	CdsP	FliK
SctW	Switch regulator	InvE	SsaL	YopN-TyeA	SepL	MxiC	PopN	CopN	-
-	Switch regulator	-	SpiC	-	SepD	-	-	-	-

In the context of *Salmonella* Typhimurium, it is important to note the different types of T3SS and their roles in infection. *Salmonella* Typhimurium contains three T3SS, including one flagellar T3SS and two virulence-associated T3SS for different phases of infection. The two virulence-associated T3SS are encoded on *Salmonella* pathogenicity islands 1 and 2 (SPI-1 and SPI-2). Pathogenicity islands are discrete chromosomal regions encoding gene sets responsible for many virulence properties of *S. enterica* (Groisman and Ochman, 1996) and are thought to have been acquired by horizontal gene transfer (Ochman, Lawrence and Groisman, 2000). SPI-1 T3SS facilitates the invasion of intestinal epithelial host cells, while SPI-2 T3SS functions after internalization, with bacteria operating inside a *Salmonella*-containing vacuole (Büttner, 2012).

The injectisome base anchors the structure to the bacterial cell envelope, forming concentric membrane rings from SctC, SctD, and SctJ. The export apparatus comprises five proteins, SctRSTU, which assemble into a helical complex above the inner membrane, and the major export apparatus protein SctV (Wagner *et al.*, 2018).

The helical needle filament, composed of over 100 SctF molecules, connects to the export apparatus through the needle adapter SctI (Marlovits et al., 2006; Broz et al., 2007; Dietsche et al., 2016; Wagner et al., 2018). Its 20 Å inner diameter permits only unfolded substrates to pass through (Loquet *et al.*, 2012). SctA forms the pentameric needle tip complex, while the translocators SctB and SctE create the translocon complex that inserts into the target cell membrane (Wagner *et al.*, 2018). Cytoplasmic components comprise the sorting platform, which works with chaperones to sequentially load appropriate substrates onto the export apparatus, ensuring secretion hierarchy in type III secretion (Lara-Tejero *et al.*, 2011).

For a successful infection, the T3SS follows a strict secretion hierarchy, which ensures that substrates are secreted in a specific order. Regulatory mechanisms, such as transcriptional, post-transcriptional, translational, and

conformational switching processes, tightly control secretion in a temporal and hierarchical manner (Deane *et al.*, 2010).

In *Salmonella* SPI-1 T3SS, an upstream regulatory system controls the expression and functionality of the master regulator HilA. This system involves transcription regulators HilC, HilD, and RtsA, which form a “regulatory triade”, capable of inducing expression of each other as well as *hilA*. Once HilA is induced, it activates the expression of structural genes (Ellermeier, Ellermeier and Slauch, 2005). Alongside these transcriptional regulators, cytoplasmic secretion regulators, such as InvE, are also crucial for establishing a hierarchy of substrate secretion and ensuring a coordinated process.

2.3 SPI-1 T3SS: regulation of secretion hierarchy

The secretion hierarchy describes distinct stages of assembly and secretion that follow a strict sequential order. The process of needle assembly, a form of secretion itself, must be completed before a translocon pore can be formed in the host cell membrane. Only following the formation of this pore can the injection of effector proteins into the target cells proceed. The fulfillment of specific requirements permits switching to the next stage. A correct sequence of these steps is crucial for a successful infection, characterized by the injection of effectors into the host cells’ cytoplasm, ultimately resulting in the typical symptoms of salmonellosis in humans (reviewed in Deane et al., 2010; Büttner, 2012; Portaliou et al., 2016; Deng et al., 2017).

There are three classes of secretion substrates: early, intermediate, and late. The two molecular switches facilitate the progression to the next phase of secretion (see Figure 2).

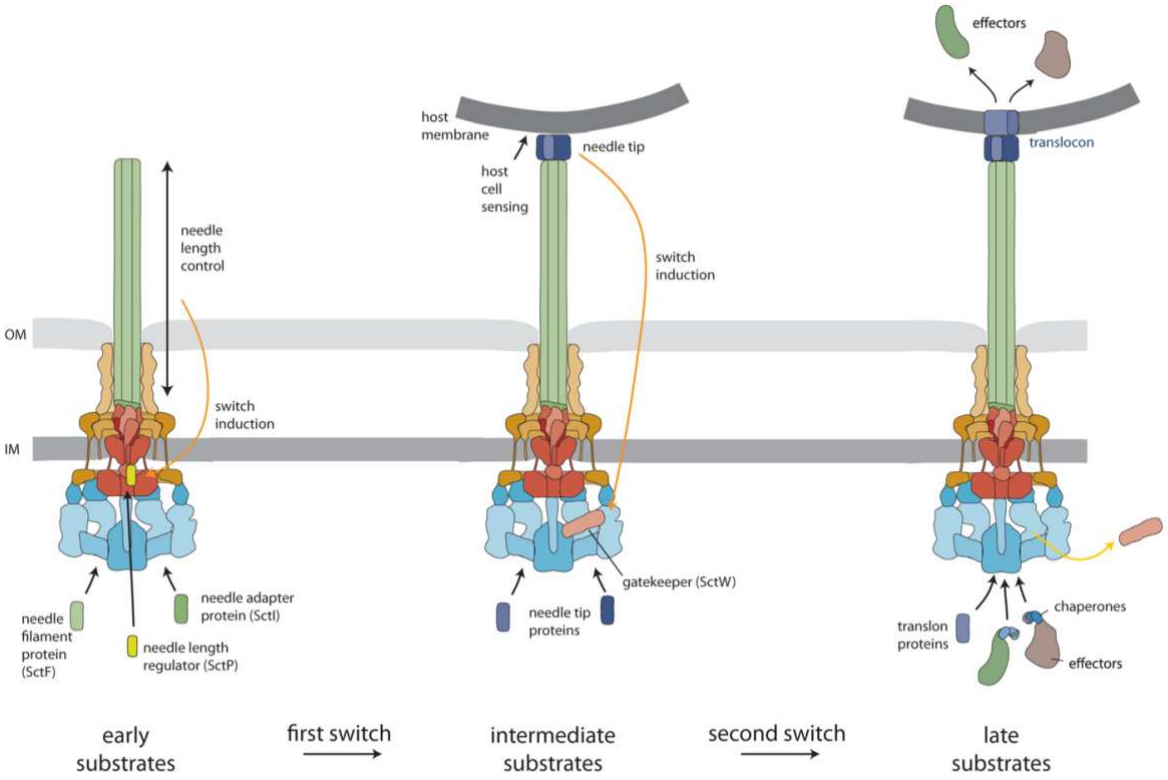

Figure 2 **Schematic overview of substrate specificity switching between the different substrates.** OM: outer membrane, IM: inner membrane. (modified from Wagner et al., 2018)

Despite similarities between flagellar and virulence-associated T3SS, particularly in the initial stages of assembly, flagellar T3SS distinguish between only early and late substrate classes and some differences in substrate specificity switching have been proposed (Chevance & Hughes, 2008; Guse et al., 2021).

Early substrates, which include the needle filament protein SctF, the needle adapter protein SctI, and the needle-length control or ruler protein SctP, are the first molecules to travel through the export apparatus and are secreted upon completion of the base (Kimbrough and Miller, 2000; Kubori *et al.*, 2000; Sukhan *et al.*, 2001a). Once the needle is formed under strict regulatory control establishing the correct needle length, the complete injectisome is assembled (Journet *et al.*, 2003). Substrate switching occurs, with the autocleavage of the cytoplasmic domain of the switch protein SctU being a prerequisite for this first switch, shifting secretion from early to intermediate substrates by altering the specificity of the export apparatus (Monjarás Feria *et al.*, 2015; Yu *et al.*, 2018).

Intermediate substrates, the translocators, include the needle tip SctA and the hydrophilic proteins SctB and SctE, that form a pore in the host cell membrane by oligomerization.

Host cell contact is suggested to be sensed either chemically or mechanically (Deng *et al.*, 2005a; Wagner *et al.*, 2018). Signal transmission to the cytoplasmic side of the T3SS then initiates the second switch from secretion of intermediate substrates to effector secretion, although the exact molecular mechanisms of signal transduction remain to be elucidated (Deng *et al.*, 2017). Subsequently, late substrates, the effector proteins, can travel through this translocon pore (Dickenson et al., 2013; Håkansson S, 1996). The gatekeeper SctW is thought to be a vital regulator at this stage (Portaliou *et al.*, 2016).

2.4 SctW as the T3SS gatekeeper

InvE, the SctW of the SPI-1 T3SS, was among the first proteins identified as necessary for *S.* Typhimurium invasion of host cells (Ginocchio, Pace and Galán, 1992). The concept of SctW as the so-called gatekeeper protein emerged later from experiments of functional knockouts of the *sctW* gene: The absence of SctW did not affect early secretion and needle formation (Sukhan *et al.*, 2001b) but resulted in reduced or abolished intermediate secretion and mostly increased late secretion in EPEC SepL (Deng *et al.*, 2004, 2005b; O'Connell *et al.*, 2004), EHEC SepL (Kresse *et al.*, 2000; Wang *et al.*, 2008), *Yersinia* TyeA/YopN (Iriarte *et al.*, 1998), *Shigella* MxiC (Martinez-Argudo and Blocker, 2010), *Salmonella* SPI-1 InvE (Kubori and Galán, 2002), and SPI-2 SsaL (Yu *et al.*, 2010). Other experiments only reported enhanced secretion of effector proteins in knockouts of *Yersinia tyeA/yopN* (Forsberg *et al.*, 1991; Boland A, 1996) and *Shigella mxiC* (Botteaux *et al.*, 2009). One study reported unaffected secretion of translocators in the ∆*mxiC* mutant (Botteaux *et al.*, 2009).

Based on PSI-BLAST, evolutionary analysis, and functional homologies, it was proposed that all these proteins are homologs that belonging to the same gatekeeper family (for an overview of the SctW homologs refer to Table 2).

Interestingly, although SctW homologs mostly exist as a single protein, in some species, they occur as two separate polypeptide chains (as in the case of Yersinia TyeA/YopN) (Pallen, Beatson and Bailey, 2005). The overall structure of the gatekeeper family is well conserved, with the core domain consisting of multiple alpha-helices (Schubot *et al.*, 2009; Nawrotek *et al.*, 2014; Burkinshaw, Souza and Strynadka, 2015). Two functional regions could be identified: an N-terminal secretion signal and a chaperone binding site. The structure is typical for so-called hub proteins that coordinate processes by interacting with multiple molecules (Schubot et al., 2005, Deane et al., 2008a; Kim et al., 2013). No SctW homolog was identified in flagellar T3SS.

Table 2 **Overview of SctW homologs** in the species relevant for this study

Unified nomenclature	***Salmonella* spp.**		***Yersinia* spp.**	**EPEC and EHEC**	***Shigella* spp.**	***P. aeruginosa***	***Chlamydia* spp.**
	SPI-1	**SPI-2**					
SctW	InvE	SsaL	YopN-TyeA	SepL	MxiC	PopN	CopN

While earlier studies located the gatekeeper on the bacterial cell surface (Forsberg *et al.*, 1991; Iriarte *et al.*, 1998; Kresse *et al.*, 2000), later studies identified SctW as an exclusively cytoplasmatic protein (Kubori and Galán, 2002; O'Connell *et al.*, 2004; Yu, Liu and Holden, 2004).

Suitably for its structure, SctW homologs have been reported to interact with a multitude of partners (see Figure 3). These include parts of the T3SS like the ATPase, the needle adapter, and the needle length regulator (Botteaux et al., 2009; Cherradi et al., 2013; Shaulov et al., 2017), different translocator chaperones (Kubori and Galán, 2002; Silva-Herzog *et al.*, 2011; Cherradi *et al.*, 2013), its own chaperone (complex) (Ferracci *et al.*, 2005; Younis *et al.*, 2010; Portaliou *et al.*, 2017), a gene expression regulator (Younis *et al.*, 2010), and an effector (Wang *et al.*, 2008). However, not all these interaction partners have homologs in other species (Shen and Blocker, 2016).

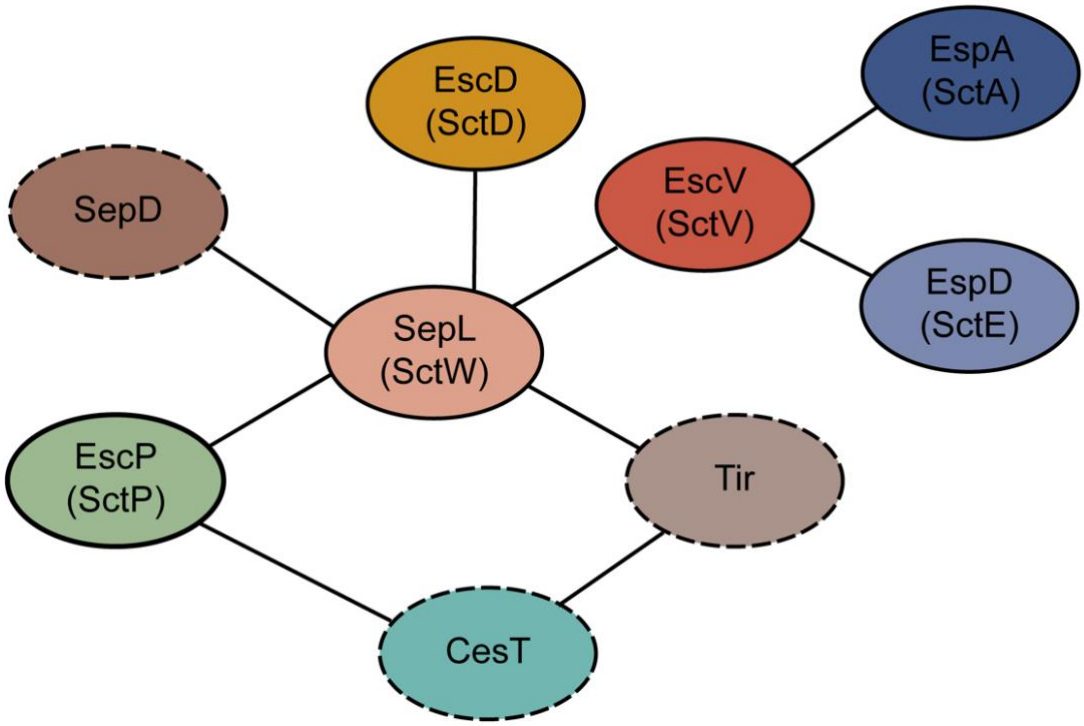

Figure 3 **Interaction network of SctW found in *E. coli*.** Unified nomenclature of *E. coli* homologs is put in parentheses, except for the gatekeeper chaperone SepD, effector Tir and its chaperone CesT which have no direct homologs (dashed lines). Additionally, SepL was shown to bind needle length regulator EscP, inner membrane ring protein EscD, and major export protein EscV, which in turn interacts with the needle tip EspA, and translocon pore protein EspD. (Modified after Gaytán et al., 2018)

Experiments suggest that SctW interacts with the major export apparatus protein SctV, serving as a binding platform for both the regulatory gatekeeper and substrate-chaperone complexes. In *Pseudomonas,* the gatekeeper Pcr1 bound to the SctV-homolog PcrD (Lee *et al.*, 2014); the C-terminus of *Shigella* SctW, MxiC, interacted with MxiA, a major export apparatus protein homolog (Shen and Blocker, 2016); in EPEC, the SepL gatekeeper protein associated with $EscV_C$ (Portaliou *et al.*, 2017; Gaytán *et al.*, 2018); and in the *Salmonella* SPI-2 T3SS, SsaL likely docked to SsaV (Yu *et al.*, 2018).

It was proposed that EPEC SctW, SepL, performs several different functions that can be separated from one another, including targeting of substrates to the membrane-associated T3SS (receptor function) and regulating translocator and effector secretion (secretion regulation function) (Wang *et al.*, 2008; Portaliou *et al.*, 2016).

The secretion phenotype of SctW homologs, with repressed intermediate secretion and increased late secretion, suggests a dual purpose of the gatekeeper: SctW appears to be required for translocator release but prevents the premature secretion of effectors. It is proposed that SctW acts as an adapter protein between chaperone-intermediate substrate complexes and the cytoplasmic domain of SctV by promoting their interaction, while simultaneously repressing the affinity of the T3SS for chaperone-effector complexes (Younis *et al.*, 2010; Portaliou *et al.*, 2016; Yu *et al.*, 2018).

In *Salmonella* SPI-2, the export gate did not interact with intermediate substrates in the absence of gatekeeper InvE. It was therefore suggested, that InvE facilitates loading of chaperone-translocator complexes onto the sorting platform, the C-ring with the ATPase components (Lara-Tejero *et al.*, 2011; Kim *et al.*, 2013). The structural basis for the repression of effector secretion is not yet known: SctW could either allosterically change SctV binding sites or occlude these to sterically prevent effector-chaperone binding (see Figure 4). After host cell sensing, release of SctW from SctV is triggered, and an affinity switch takes place, now favoring late substrates for secretion and translocation (Portaliou *et al.*, 2017).

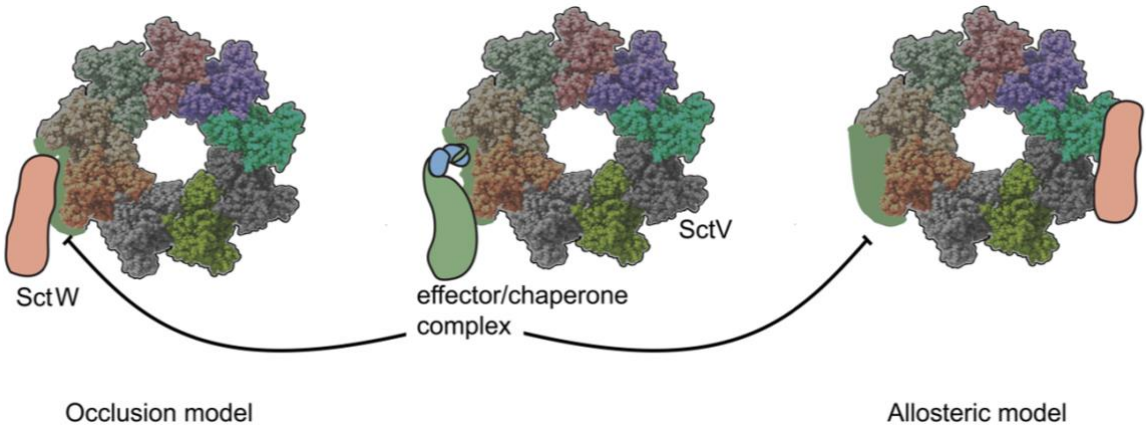

Figure 4 **Schematic overview of possible SctW gatekeeper mechanism.** Occlusion (left) and allosteric (right) model of SctW repression of effector targeting. (Modified after Portaliou et al., 2016).

Different mechanisms of disengagement of SctV and SctW are being discussed, including SctW secretion, dissociation of the SctV-SctW-chaperone complex, or SctW detachment (Portaliou *et al.*, 2017). Secretion was reported for the homologs YopN (Sundberg and Forsberg, 2003), MxiC (Botteaux *et al.*, 2009; Cherradi *et al.*, 2013; Roehrich *et al.*, 2017), and CopN (Archuleta *et al.*, 2011; Silva-Herzog *et al.*, 2011). In *Salmonella* T3SS, there is no evidence for secretion of the gatekeeper protein. Instead, data suggest that InvE and SsaL get degraded in the cytoplasm (Kubori and Galán, 2002; Yu *et al.*, 2010), possibly after complex dissociation (Yu *et al.*, 2018). For SepL in *E.* coli, different mechanisms are being discussed and remain to be further elucidated (Younis *et al.*, 2010; Portaliou *et al.*, 2017; Shaulov *et al.*, 2017).

The current data does not support one unified regulatory model for the second switch and gatekeeper function. Although there are prominent functional similarities between the proteins of the SctW family, subtle differences and distinct characteristics of each protein might be crucial for fine-tuning to the specific requirements in each species. Different effector proteins, secretion triggers and host environments might preclude a completely universal gatekeeper mechanism (Deane *et al.*, 2010).

Still, an interaction between the gatekeeper protein and the major export apparatus protein was suggested to be central to the mechanism behind the second switch in several species (Lara-Tejero *et al.*, 2011; Portaliou *et al.*, 2017; Yu *et al.*, 2018). Therefore, this interaction between SctW and SctV is potentially a key common denominator for the substrate specificity switching from intermediate to late secretion substrates.

2.5 InvE-InvA interaction for secretion regulation

The major export apparatus protein SctV forms a nonameric ring around the inner membrane proteins SctRSTU, with each SctV protomer containing 8 predicted transmembrane helices in an N-terminal transmembrane domain (TMD). (Worrall, Vuckovic and Strynadka, 2010; Abrusci *et al.*, 2013). The large cytoplasmic C-terminal domain is divided into four subdomains (SD 1-4),

conserved across species. Rearrangement of these C-terminal subdomains leads to an “open” conformation of the export apparatus, potentially regulating interaction with other T3SS components (Deane *et al.*, 2008b). SctV plays a crucial role in controlling the hierarchy of substrate selection and possibly energizing secretion as a proton channel (Majewski *et al.*, 2020).

Several interactions sites between SctW and SctV have been identified. In EPEC, peptide array signals were mapped on the EscV monomer structure model and a nonameric ring model from the *Shigella* MxiA structure (Abrusci *et al.*, 2013). Gatekeeper SepL was found to bind the external surface of EscV, where two protomers form a groove with two adjacent binding sites. The interacting residues in SepL were mainly localized in subdomains (SD) 2 and SD 3 (Portaliou *et al.*, 2017). Comprehensive mutational analysis in the *S.* Typhimurium SPI-2 T3SS identified regions in the SD 4 of SsaV that phenocopied Δ*ssaL* mutants regarding secretion and host cell invasion. One of the mutations identified in the *S*. Tymphimurium SPI-2 T3SS was tested in InvA, the SPI-1 SctV homolog, yielding comparable results (Yu *et al.*, 2018). In a flagellar T3SS, a common binding site of chaperone-substrate complexes on the SctV-homolog FlhA was identified in crystal structures. This highly conserved binding site is at the interface of SD 1 and SD 2 but is not conserved in virulence-associated T3SS (Xing *et al.*, 2018). Notably, the interaction sites identified in the Portaliou and Yu studies do not overlap. Furthermore, conclusive *in vivo* or *in vitro* evidence for a physical interaction between SctW and SctV is still lacking.

In conclusion, the relationship between the gatekeeper SctW and the major export apparatus protein SctV remains poorly understood, although it is very likely that SctW binds to the clefts on the lower inner surface between SsaV subunits. Therefore, investigating the relationship between InvE and InvA in *Salmonella* SPI-1 T3SS presents a promising approach to gain further insight into the gatekeeper’s role in the secretion of translocators and effector proteins.

3 Aim of this work

This work aimed to structurally characterize the interaction between InvE and InvA in the *Salmonella* SPI-1 T3SS using *in vivo* photocrosslinking. The goal was to understand how the gatekeeper protein InvE influences secretion and to propose a mechanism of action for substrate specificity switching between the secretion of intermediate and late substrates.

3.1 Experimental strategy

To achieve the objectives outlined above, the following experimental strategies were employed:

First, plasmid-based complementation of InvE was established, and a functional epitope-tagged variant of InvE was engineered to facilitate complex purification and interaction analysis.

Next, functionality of T3SS was assessed by measuring secretion function with a TCA-based T3S assay, and a luciferase based T3S assay. For the latter, bacterial strains harboring C-terminal NanoLuc luciferase fusions of translocator SipD or effector SipA were utilized to allow for fast quantitative analysis of intermediate and late secretion. (Westerhausen *et al.*, 2020).

Finally, the predicted interaction sites of SctW and SctV (Portaliou *et al.*, 2017; Xing *et al.*, 2018; Yu *et al.*, 2018) were tested by site-specific *in vivo* photocrosslinking in *Salmonella* (Singh and Wagner, 2019). This experimental setup was based on the artificial amino acid *para*-Benzoyl-phenylalanine (pBpa), which is a phenylalanine derivative with an additional benzophenone group (see Figure 5B). The plasmid pSup-*p*Bpa, carrying the genes for an aminoacyl-tRNA synthetase and its amber suppressor tRNA that gets loaded with *p*Bpa, was introduced (Liu *et al.*, 2007). Amber mutations were introduced at selected sites of *invE* and *invA* where protein-protein interactions were expected. Additionally, these bacterial strains carried the pSup-*p*Bpa plasmid.

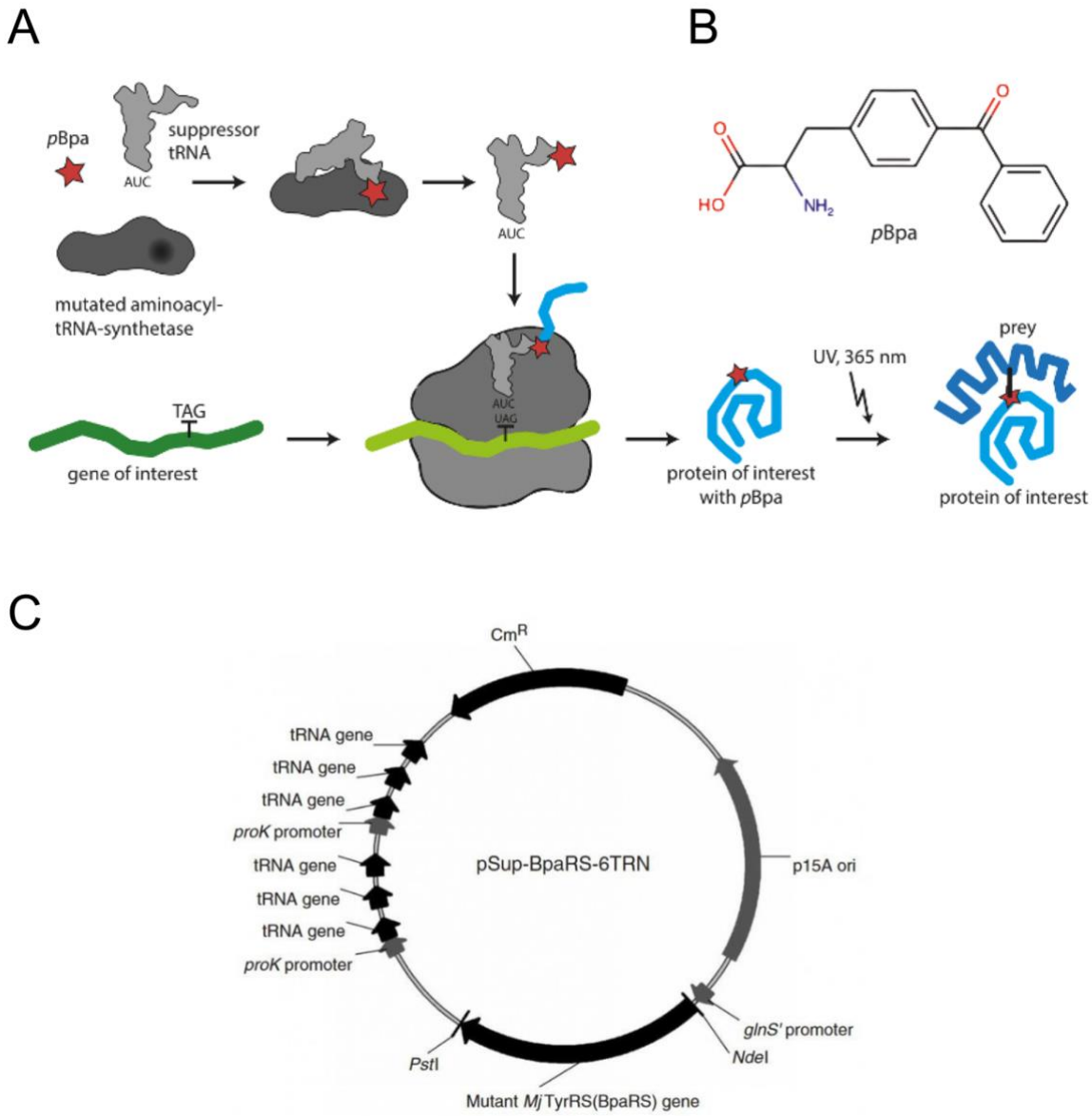

Figure 5 **Schematic representation of site-specific *in vivo* photocrosslinking. (A)** An amber stop codon (AUC) is introduced into the gene of interest (this study: *invE* or *invA*). The suppressor tRNA is charged with *p*Bpa by a mutated tRNA-synthetase and *p*Bpa gets integrated at the position of the amber stop codon. In the case of protein-protein interaction at the specific tested position, UV irradiation results in crosslinks between these proteins. **(B)** Chemical structure of *para*-Benzoyl-phenylalanine. **(C)** Plasmid map of pSup-BpaRS-6TRN (Ryu and Schultz, 2006), License: CC BY 4.0

Upon UV irradiation at 365 nm, crosslinks were established between the benzophenone group of *p*BpA and close-by amino acids from interaction partners. The now covalently bound protein-protein complexes could then be analyzed by SDS PAGE and Western blot using epitope tags.

4 Material and Methods

4.1 Chemicals, enzymes, buffers, and media

All chemicals and enzymes were purchased from AppliChem (Darmstadt), Becton Dickinson (Franklin Lakes, USA), Carl Roth (Karlsruhe), Merck (Darmstadt), New England Biolabs (Frankfurt am Main), SERVA (Heidelberg), Sigma-Aldrich (St. Louis, Missouri, USA), or VWR (Radnor, Pennsylvania, USA), if not stated otherwise. All media, reagents, buffers, and solutions used in this study's experiments are specified in Table 3.

4.2 Antibodies

All antibodies used in this study can be found in Table 4. Before use, they were diluted in TBS-T. The secondary antibodies are conjugated to DyLight 680 and DyLight 800 4x PEG, respectively. These fluorophores allow detection by a LI-COR Odyssey system (ODY-3191).

4.3 Bacterial strains and growth conditions

Salmonella enterica subspecies *enterica* serovar Typhimurium (*S.* Typhimurium) and *Escherichia coli* (*E. coli*) strains (Table 5) were grown in either liquid LB medium at 37 °C, 180 rpm, or on LB agar medium at 37 °C, unless mentioned otherwise. Respective antibiotics were added to all media in the following concentrations: ampicillin (Amp): 100 µg/ml, chloramphenicol (Cm): 25 µg/ml, kanamycin (Kan): 25 µg/ml, streptomycin (Strep): 50 µg/ml, and tetracycline (Tet): 12.5 µg/ml. Additional 100 µg/ml diaminopimelic acid (DAP) were added to the media of *E. coli* β2163. Gene expression of the SPI-1 encoded T3SS was induced by growing *S.* Typhimurium in liquid LB-NaCl medium with low aeration. The bacterial strains were kept on LB agar platesat 4 °C for up to four weeks. For long term storage, the bacterial cells were frozen in 1.5 ml stock medium at -80 °C.

4.4 QuikChange site-directed mutagenesis

Amber stop codon point mutations were introduced in target genes by QuikChange site-directed mutagenesis (Agilent Technologies), to facilitate *in vivo* photocrosslinking experiments. PCR was performed with KOD Hot Start DNA polymerase and QC primers (Table 7) following the QuikChange protocol by Agilent Technologies. Afterwards, the PCR product was digested with 1 µl of 20,00 U/mL DpnI at 37 °C for at least 1 h to remove template DNA. Chemically competent *E. coli* NEB5α for pT10 plasmid and *E. coli* pir116 for pSB890 derived plasmids were transformed with 5 µl of the reaction product by heat shock transformation, respectively. Plasmids were extracted with the QIAprep Spin Miniprep Kit (Qiagen) and positive mutants were identified using sequencing analysis with 14 µl plasmid and 1 µl primer (Eurofins Genomics). For pSB890 derived plasmids, *E. coli* β2163 Δ*nic35* were transformed by electroporation. The bacteria were then stored ins stock medium at -80°C.

4.5 Gibson cloning

Vector and insert DNA fragments were used to construct plasmids using Gibson assembly (Gibson *et al.*, 2009). PCR was performed using Q5 Hot Start High-Fidelity DNA polymerase and Gibson primers (Table 7) to amplify inserts and vector DNA. Afterwards, the PCR product was digested with 1 µL of 20,00 U/mL DpnI at 37 °C for at least 1 h and analyzed on a 1% (w/v) agarose gel in TAE buffer. PCR products were assembled in 12.5 µl Gibson master mix containing DNA ligase, DNA polymerase, and T5 exonuclease for 1 h at 50 °C. Subsequently, for pT10 plasmids, chemically competent *E. coli* NEB5α were transformed with 5 µl of the reaction product. For pSB890, *E. coli* pir116 were transformed, respectively. Plasmids were extracted with the QIAprep Spin Miniprep Kit (Qiagen) and positive mutants were identified using sequencing analysis with 14 µl plasmid and 1 µl primer (Eurofins Genomics). For pSB890 derived plasmids, *E. coli* β2163 Δ*nic35* were transformed by electroporation. The bacteria were then stored in stock medium at -80 °C.

4.6 Electrotransformation and heat shock transformation

Table 6 lists the plasmids used in this study, which were either introduced into *S.* Typhimurium strains or *E. coli* β2163 by electroporation. Cells were made electrocompetent by washing the cells three times with ice cold 10 % (v/v) glycerol (Dower, Miller and Ragsdale, 1988). If not directly used for electrotransformation, the aliquots were frozen in liquid nitrogen and stored at -80 °C. For electrotransformation, electrocompetent cells were mixed with 1 µl plasmid DNA and precooled electroporation cuvettes (BIO-RAD). Electroporation was performed with the Eppendorf Multiporator at 1.8 kV, 200 Ω and 25 µF.

For heat shock transformation, cells were thawed for 5-10 minutes on ice. Then, the cells were mixed with 1 µl of plasmid DNA and kept on ice for an additional 30 minutes. The cells were then heat-shocked for 30 seconds at 42 °C, followed by an 2 minute incubation on ice to help the cells recover.

In both cases, transformed bacteria were resuspended in SOC medium and after shaking incubation at 37 °C, were plated on LB agar.

4.7 Allelic exchange

To introduce chromosomal mutations into *Salmonella* strains, allelic exchange mutagenesis was performed. The tetracycline resistant suicide plasmids used for this purpose encode the mutated gene of interest with about ± 1000 bp flanking regions that are equivalent to the chromosomal context. Cloning and propagation of the pSB890 plasmid was performed in *E. coli* pir116 cells, which express the π-protein initiating the replication through the R6K origin (Kvitko *et al.*, 2012). The donor strain of the suicide plasmid was *E. coli* β2163 Δ*nic35*, which can mate with *Salmonella* strains, thereby transferring the plasmid. The recipient *Salmonella* strain was grown overnight (o/n) in LB/Strep, and the *E. coli* β2163 were grown in LB/Tet/DAP. Equal amounts of both o/n cultures were then mixed, spun down at 6000 rpm (Eppendorf MiniSpin, rotor F-45-12-11) for 2 min at room temperature (RT) and washed with 1 ml LB/DAP to get rid of antibiotics. The sample was centrifuged again, the supernatant removed, and

the cells were resuspended in in 30 µl LB/DAP and spotted in LB/DAP agar medium. Cells were grown for 8 h at 37 °C, during which the suicide plasmid was transferred to *Salmonella* via mating. The plasmid was integrated into the *Salmonella* chromosome via homologous recombination resulting in merodiploids. It was then selected for merodiploids via growth on LB/Strep/Tet. Individual merodiploid colonies were grown in 5 ml LB/Strep at 37 °C under agitation for 24 h. Cultures were diluted 1:1000 by transferring 1 µl of cells in 1 ml of LB medium and 100 ml of this dilution were plated on a counterselective sucrose agar plate with Strep and incubated at 30 °C for 12-16 h. This step selects for clones that have lost the suicide plasmid, since this plasmid contains the marker *sacB*, which codes for the enzyme levansucrase that metabolizes sucrose to the cytotoxic product levan. Losing the plasmid results in either wild type allele or the integration of the desired mutation. To identify the mutants, colony PCR was performed of bacteria that did not grow in the presence of tetracycline. To confirm the results, PCR products were purified with the QIAquick PCR Purification Kit by QIAGEN according to manufacturer's protocol with the modification of elution in 40 µL EB buffer and analyzed by sequencing (Eurofins Genomics).

4.8 TCA based secretion assay

Bacteria were grown o/n in 3 ml LB-NaCl media and all respective antibiotics. Fresh cultures were started in the morning by adding 300 µl of o/n culture to 10 ml LB-NaCl media with respective antibiotics and 500 µM rhamnose for gene expression, resulting in an OD_{600} of about 0.05. After growing the cultures for a fixed time of 6 h, 0.5 ODU whole cells (wc) and 1.8 ml bacterial culture were harvested by centrifugation (10000 x *g*, 2 min, 4 °C). The whole cells were resuspended in 75 µl SB buffer and heated for 10 min at 50 °C. The supernatant (sn) of the culture was filtered through a 0.2 µm membrane filter (Acrodisc HT Tuffryn 0.2 µm 25 mm, Pall). Then, 0.1 % (w/v) sodium deoxycholate and 10 % (w/v) trichloroacetic acid (TCA) were added to the supernatant, and the sample was incubated for 30 min at 4 °C. Afterwards, the

precipitated proteins were pelleted by centrifugation (20000 x *g*, 20 min, 4 °C), resuspended in 1 ml ice-cold acetone and incubated for 5 min at 4 °C. The proteins were then pelleted by centrifugation (20000 x *g*, 15 min, 4 °C) again, and the supernatant was discarded. The pellets were resuspended in 40 µl SB buffer and boiled for 10 min at 95 °C. wc (0.1 ODU) and sn proteins (20 µl) were analyzed by SDS PAGE and immunoblotted against the early substrate InvJ and the intermediate substrate SipB.

4.9 NanoLuc secretion assay

NanoGlo® Luciferase Assay System (Promega) based secretion assays enable fast quantitative secretion analysis of NL-tagged T3SS substrates. O/n cultures grown in LB-NaCl were diluted to an OD_{600} of about 0.05, as described in 3.8, in LB-NaCl with respective antibiotics and 100 µM rhamnose for pT10 and 0.05 % (w/v) arabinose for pBAD24, respectively. The cells were then grown for 5.5 h at 37 °C. Afterwards, bacterial cells and supernatant were separated by centrifugation (10000 x *g*, 2 min, 4 °C). For the NL working solution, NanoGlo® luciferase substrate was mixed with the NanoGlo® luciferase buffer (Promega) in a 1:50 ratio. 25 µl of the supernatant was transferred to a Nunc® MaxiSorpTM 384 well plate (Thermo Fisher Scientific) and 25 µl of the working solution was added. The mixture was incubated for 5 min at RT. NanoLuc produces high intensity luminescence by oxidising its substrate furimazine, which was then measured by Tecan Spark® microplate reader (parameters: attenuation auto, integration time 100 ms or 1,000 ms).

4.9.1 Statistical Rationale

To reduce systematic errors, experiments were repeated, and samples were measured multiple times. Independent, biological replicates were carried out to ensure biological and analytical reliability. Technical replicates were conducted for quality control of the experimental protocols and the accuracy of the measuring instruments.

Background luminescence was measured and subtracted from the dataset. Outliers were identified by ROUT method (Q = 1 %) in GraphPad. For each biological replicate, samples were normalized to the wild type to allow for better comparison. The mean of the normalized luminescence of all the samples for one experiment was then plotted as a bar chart with error bars representing the standard deviation. Statistical analysis and visualization were performed using Prism GraphPad (version 9.4.1).

4.10 *In vivo* Photocrosslinking

A prerequisite for site specific *in vivo* photocrosslinking was to transform *S.* Typhimurium with pBAD24-*hilA*, pSup-*p*Bpa, and a pT10 plasmids with the desired mutation. HilA is the main transcriptional regulator of SPI-1 and ensured high levels of T3SS within each cell by promoting expression of the invasion genes.

Bacteria were grown o/n in 3 ml LB-NaCl media supplemented with all appropriate antibiotics (Strep, Tet, Cm, Amp, Kan) and diluted in the morning to an OD_{600} of about 0.05, as described above. For the day culture, only Amp of all antibiotics was used, since the low copy number plasmids pT10 and pSup-*p*Bpa are stable enough and hence, do not require antibiotics for shorter periods of growth. Gene expression was induced with 500 µM rhamnose for pT10 and 0.05 % (w/v) arabinose for pBAD24, respectively. Additionally, *p*Bpa (Bachem, Bubendorf, Switzerland) was dissolved in 1 M NaOH and added to the culture to a final concentration of 1 mM while shaking. Cultures were grown for 6 h at 37°C, 180 rpm. Afterwards, 8 ODU were harvested by centrifugation (4000 x *g*, 3 min, 4 °C). In case of a parallel secretion assay, 1.8 ml of 500 µl of the culture were taken for TCA precipitation or NL assay, respectively (see 3.8 and 3.9). The pelleted cells were washed with 3 ml ice cold PBS and centrifuged again (4000 x *g*, 3 min, 4 °C), before resuspension in 2 ml ice cold PBS. For crosslinking of the proteins, half of the sample was irradiated with ultraviolet light (UV) at λ = 365 nm in a CELLSTAR® 6 well cell culture plate (Greiner Bio-One) for 30 min (+ UV), while the other half of the sample was left untreated (-

UV). Hereafter, the samples were centrifuged (10000 x *g*, 2 min, 4 °C) and the supernatant was discarded. The cells were then subjected for crude membrane preparation, or frozen at –20 °C and subjected to SDS or BN PAGE, afterwards.

4.11 Crude membrane preparation

Pellets corresponding to 4 ODU were resuspended in 750 µl buffer K with additives, added to 500 µl glass beads (150-212 µm, acid-washed, Sigma-Aldrich) in 2 ml screw cap tubes. After incubation for 30 min at 4 °C, samples were lysed in a bead mill (SpeedMill PLUS, Analytik Jena) for 2 min in continuous mode. Following centrifugation (1,000 x *g*, 1 min, 4 °C), the supernatant was transferred to a new 1.5 ml tube and washed by adding 1 ml buffer K without additives and subsequent centrifugation (1,000 x *g*, 1 min, 4 °C). Afterwards, the supernatant was transferred to the same tube as before. Samples were then centrifuged (10,000 x *g*, 10 min, 4 °C) to get rid of cell debris and remaining beads. The supernatant was transferred to ultracentrifugation tubes and crude membranes were isolated from the supernatant by ultracentrifugation (52,000 x *g*, 50 min, 4 °C, Beckman Coulter Optima MAX with a TLA55 rotor). Finally, supernatant was aspirated, and the crude membranes were then frozen at –20 °C until usage or directly subjected to SDS and BN PAGE analysis. For SDS PAGE, 4 ODU of crude membranes were resuspended in 40 µl 1x SB buffer and heated for 10 min at 50 °C. The gel was loaded with 20 µl, corresponding to 2 ODU.

4.12 SDS PAGE

Denatured proteins were separated by their molecular weight on ServaGel TG Prime 8-16 % precast gels (Serva) with Precision Plus Protein All Blue standards (Bio-Rad) as a molecular weight reference. SDS gels were run in 1 x SDS running buffer at 110 V for 15 min, followed by an additional 85 min at 210 V, in a SERVA BlueVertical™ electrophoresis chamber.

4.13 BN PAGE

For BN PAGE, 8 ODU were resuspended in 90 µl 1 x PBS and solubilized in 1 % (w/v) lauryl maltose neopentyl glycol (LMNG) (Anatrace) for 60 min at 4 °C, shaking at 500 rpm. To remove unsolubilized material, sample was centrifuged (20,000 x g, 30 min, 4 °C). 30 µl of the supernanant were mixed with SB buffer and subjected to SDS PAGE (see 3.12) and 45 µl were mixed with 5 µl of 1x blue native loading buffer and used for BN PAGE. The native protein complexes were separated by their molecular weight on NativePAGE™ 3-12 % Bis-Tris protein gels (Invitrogen). Gels were run in 1x BN anode buffer and 1x BN cathode buffer I at 130V, 200 mA, for 1 h at 4 °C in a SERVA BlueVerticalTM PRiMETM electrophoresis chamber. After that, the 1x BN cathode buffer I was exchanged with 1 x BN cathode buffer II and electrophoresis was continued at 300 V, 200 mA, for 1.5 h at 4 °C. Eventually, the BN gels were equilibrated in SDS running buffer for 20 min in preparation for Western blot analysis.

4.14 Western blot analysis and immunodetection

Following SDS or BN PAGE, proteins were blotted on polyvinylidene difluoride (PVDF) membranes (BIO-RAD) using a wet blot protocol, in 1x transfer buffer. For the transfer, either the CriterionTM Blotter (Bio-Rad) was used at 35 V for 3.5 h, or the Trans-BlotTM Cell (Bio-Rad) at 60 V for 3 h, both times at 4 °C. For BN gels, the membrane was washed several times with 100 % methanol to remove residual Coomassie, before it was subjected to immunodetection.

After blotting, the membrane was incubated in 1 x Blue Block PF (Serva) for 1 h at RT to block unspecific binding sites. The membranes were rinsed with 1 x TBS-T and incubated with a primary antibody (Table 4) for 1 h at RT or o/n at 4 °C. Then, the membrane was washed three times with 1 x TBS-T for 10 to 15 min and afterwards incubated with the secondary antibody (Table 4) for 1 h at RT or o/n at 4 °C. After another three washing steps with TBS-T, the membrane was transferred and stored in TBS. A shaker was utilized for all these steps.

Scanning of the membranes was performed with LI-COR Odyssey (ODY-3191) and image analysis was performed with Image Studio 2.1 (LI-COR).

4.15 Bioinformatics

To predict the nonameric InvA structure, AlphaFold was used (Jumper et al., 2021; Varadi et al., 2022). For prediction of the cytoplasmic region, amino acids 357-685 of InvA were used as inputs. Visualization was done with UCSF ChimeraX (https://www.rbvi.ucsf.edu/chimerax/).

Table 3 **Media, buffers, solutions, and gels used in this study**

Name	Recipe
Media for bacterial culture	
LB medium	5 g NaCl, 10 g tryptone and 5 g yeast extract were dissolved in 1 l H_2O and autoclaved.
LB - 0.3 M NaCl medium	12.5 g NaCl, 10 g tryptone, 5 g yeast extract were dissolved in 1 l H_2O and autoclaved.
LB agar medium	6 g LB Lennox and 4.5 g agar were dissolved in 300 ml H_2O and autoclaved. Afterwards, respective antibiotics were added.
Sucrose agar medium	5 g tryptone, 2.5 g yeast extract and 7.5 g agar were dissolved in 400 ml H_2O and autoclaved. Afterwards, 100 ml sterile filtered (0.22 µm) 50 % (w/v) sucrose were added.
additives to LB agar/medium	See 4.3 Bacterial strains and growth conditions
super optimal broth (SOB) medium	40 g bacto-tryptone, 10 g yeast extract, 1 g NaCl and 0.373 g KCl were dissolved in 2 l H_2O and autoclaved. Then, sterile filtered (0.22 µm) 1 M $MgCl_2$ and 1 M $MgSO_4$ solutions were added to a final concentration of 10 mM
SOC medium	20 ml sterile filtered (0.22 µm) 1 M glucose were added to 1 l SOB medium
Stock medium	63 g glycerol and 10 g peptone were dissolved in 500 ml H_2O and autoclaved
Reagents for cloning	
5 x ISO Mix	300 µl 1M Tris-HCl pH 7.5, 30 µl 1 M $MgCl_2$, 60 µl 10 mM dNTP Mix, 30 µl 1 M DTT, 150 mg PEG 8000, 30 µl 100 mM NAD and 600 µl H_2O were mixed.
Gibson master mix	100 µl 5 x ISO mix, 0.2 µl T5 exonuclease, 6.25 µl Phusion DNA polymerase and 50 µl *Taq* DNA Ligase were mixed in 218.6 µl H_2O
Buffers	
10x PBS	80 g NaCl, 2 g KCl, 14.4 g $Na_2HPO_4 \cdot 2\ H_2O$ and 2.4 g KH_2PO_4 were dissolved in 1 l H_2O and the pH was adjusted to 7.4 with NaOH. Before use, the buffer was diluted 1:10 in H_2O
Buffer K	50 mM TEA, 250 mM sucrose and 1 mM EDTA pH 8 were dissolved in 500 ml H_2O. Then, the pH was adjusted to 7.5 with acetic acid
Buffer K with additives	750 µl buffer K mixed with 1 mM $MgCl_2$, 1 mM EDTA, 10 µg/mL DNase, 10 µg/mL lysozyme, 1x protease inhibitor cocktail
50x TAE buffer	242 g Tris base, 57.1 ml glacial acetic acid and 37.2 g EDTA were dissolved in 1 l H_2 O. Before use, the buffer was diluted 1:50 in H_2O.

SDS running buffer	30 g Tris base, 144 g glycine and 10 g SDS were dissolved in 1 l H_2O. Before use, the buffer was diluted 1:10 in H_2O
4x solubilization buffer (SB)	10 ml 0.5 M Tris-HCl pH 6.8, 5 ml 80% (v/v) glycerol, 1.6 g SDS and 10 mg bromophenol blue were filled up to 16 ml with H_2O. Before use, the buffer was appropriately diluted in H_2O and supplemented with a final concentration of 5 % (v/v) β-mercaptoethanol
6x DNA loading buffer	1.9 ml 80 % (v/v) glycerol, 20 µl Tris-HCl pH 8.8 and a small piece of bromophenol blue were added to 3 ml H_2O
10x Transfer buffer	30g Tris base, 144g glycine and 2.5g SDS were dissolved in 1l H_2O. Before use, the buffer was diluted 1:10 in H_2O supplemented with a final concentration of 10 % (v/v) methanol.
10x TBS	84g NaCl and 30g Tris base were dissolved in 1l H_2O. Then, the pH was adjusted to 8.0 with HCl. Before use, the buffer was diluted 1:10 in H_2O.
TBS-T	TBS was supplemented with 0.05 % (v/v) Tween20
Buffers for BN PAGE	
10x Anode buffer	52.3 g Bis-Tris were dissolved in 500 ml H_2O. Before use, the buffer was diluted 1:10 in H_2O
10x Cathode buffer I	44.79 g tricine (Biomol, Hamburg), 15.69 g Bis-Tris and 1 g Coomassie Serva Blue G were dissolved in 500 ml H_2O and mixed over night at 4 °C. Before use, the buffer was diluted 1:10 in H_2O
10x Cathode buffer II	44.79 g tricine (Biomol, Hamburg) and 15.69 g Bis-Tris were dissolved in 500 ml H_2O. Before use, the buffer was diluted 1:10 in H_2O supplemented with 10 % (v/v) Cathode buffer I
Blue native loading buffer	25 mg Coomassie Serva Blue G were dissolved in 450 µl 250 mM aminocaproic acid (ACA) supplemented with 50 % (v/v) glycerol

Table 4 **Antibodies used in this study.**

Antibody	Clonality	Dilution	Origin	Order	Source
α-FLAG, M2	monoclonal	1:10000	mouse	primary	Sigma-Aldrich
α-HA	polyclonal	1:1000	rabbit	primary	Sigma-Aldrich
α-SipB	monoclonal	1:1000	mouse	primary	Lab stock
α-InvJ	monoclonal	1:500	mouse	primary	Lab stock
α-StrepTagII	monoclonal	1:1000	mouse	primary	Iba Lifesciences
α-Mouse800	polyclonal	1:10000	goat	secondary	Thermo Fisher
α-Rabbit800	polyclonal	1:10000	goat	secondary	Thermo Fisher

Table 5 ***Escherichia coli*** **and** ***Salmonella*** **Typhimurium strains used in this study**. Only strains that were used in the experiments that are shown are included. All *Salmonella* strains are Strep resistant.

Name	Description	Source
Escherichia coli		
NEB5α	fhuA2Δ(argF-lacZ)U169 phoA glnV44 Φ80Δ(lacZ)M15 gyrA96 recA1 relA1 endA1 thi-1 hsdR17	Wagner lab
λpir116	endA1 hsdR17 glnV44 (= supE44) thi-1 recA1 gyrA96 relA1 Φ80dlacΔ(lacZ)M15 Δ(lacZYA-argF)U169 zdg-232 uidA::pir116	Wagner lab
β2163 Δ*nic35*	(F-) RP4-2-Tc::Mu DdapA::(erm-pir) [KmR ErmR]	Wagner lab
Salmonella enterica		
SB300	*Salmonella enterica* subspecies enterica serovar Typhimurium strain SL1344 (WT)	Wagner lab
MIB5407	SB300, Δ*rha*, Δ*ara*, SipD-NL; made with pMIB5955	This study
MIB5409	SB300, Δ*rha*, Δ*ara*, SipA-NL; made with pMIB5563	This study
MIB5481	SB300, Δ*rha*, Δ*ara*, InvA$^{HA\text{-}TEV\text{-}FLAG}$, SipD-NL; made with pMIB7289	This study
MIB5483	SB300, Δ*rha*, Δ*ara*, InvA$^{HA\text{-}TEV\text{-}FLAG}$, SipA-NL; made with pMIB7289	This study
MIB5489	SB300, Δ*invE*, Δ*rha*, Δ*ara*, SipD-NL; made with pMIB5175	This study
MIB5491	SB300, Δ*invE*, Δ*rha*, Δ*ara*, SipA-NL; made with pMIB5175	This study
MIB5507	SB300, Δ*invE*$_{complete}$, Δ*rha*, Δ*ara*, SipD-NL; made with pMIB7580	This study
MIB5509	SB300, Δ*invE*$_{complete}$, Δ*rha*, Δ*ara*, SipA-NL; made with pMIB7580	This study
MIB5529	SB300, invE^{FLAG}, Δ*rha*, Δ*ara*, SipD-NL; made with pMIB7721	This study
MIB5531	SB300, ^{FLAG}invE, Δ*rha*, Δ*ara*, SipD-NL; made with pMIB7722	This study
MIB5533	SB300, invE^{StrepTagII}, Δ*rha*, Δ*ara*, SipD-NL; made with pMIB7723	This study
MIB5535	SB300, invE^{FLAG}, Δ*rha*, Δ*ara*, SipA-NL; made with pMIB7721	This study
MIB5537	SB300, ^{FLAG}invE, Δ*rha*, Δ*ara*, SipA-NL; made with pMIB7722	This study
MIB5539	SB300, invE^{StrepTagII}, Δ*rha*, Δ*ara*, SipA-NL; made with pMIB7723	This study
MIB5565	SB300, invE^{FLAG}, Δ*rha*, Δ*ara*, Δ*invA*, SipD-NL; made with pSB3531	This study
MIB5567	SB300, invE^{FLAG}, Δ*rha*, Δ*ara*, Δ*invA*, SipA-NL; made with pSB3531	This study
MIB5571	SB300, Δ*rha*, Δ*ara*, InvA$^{HA\text{-}TEV\text{-}FLAG}$, *invE* G225X, SipD-NL, made with pMIB7790	This study
MIB5573	SB300, Δ*rha*, Δ*ara*, InvA$^{HA\text{-}TEV\text{-}FLAG}$, *invE* Q326X, SipD-NL, made with pMIB7791	This study
MIB5575	SB300, Δ*rha*, Δ*ara*, InvA$^{HA\text{-}TEV\text{-}FLAG}$, *invE* M347X, SipD-NL, made with pMIB7792	This study

MIB5577	SB300, Δ*rha*, Δ*ara*, InvA$^{HA\text{-}TEV\text{-}FLAG}$, *invE* I355X, SipD-NL, made with pMIB7793	This study
MIB5579	SB300, Δ*rha*, Δ*ara*, InvA$^{HA\text{-}TEV\text{-}FLAG}$, *invE* Y357X, SipD-NL, made with pMIB7794	This study
MIB5721	SB300, Δ*rha*, Δ*ara*, InvA$^{HA\text{-}TEV\text{-}FLAG}$, *invE* G225X, SipA-NL, made with pMIB7790	This study
MIB5723	SB300, Δ*rha*, Δ*ara*, InvA$^{HA\text{-}TEV\text{-}FLAG}$, *invE* Q326X, SipA-NL, made with pMIB7791	This study
MIB5725	SB300, Δ*rha*, Δ*ara*, InvA$^{HA\text{-}TEV\text{-}FLAG}$, *invE* M347X, SipA-NL, made with pMIB7792	This study
MIB5727	SB300, Δ*rha*, Δ*ara*, InvA$^{HA\text{-}TEV\text{-}FLAG}$, *invE* I355X, SipA-NL, made with pMIB7793	This study
MIB5729	SB300, Δ*rha*, Δ*ara*, InvA$^{HA\text{-}TEV\text{-}FLAG}$, *invE* Y357X, SipA-NL, made with pMIB7794	This study

Table 6 **Plasmids used in this study.** Only plasmids used for the experiments that are shown are listed.

Name	Description	Resistance	Source
pSB3292	pBAD24-*hilA*	Amp	Wagner lab
pSup-pBpa	Amber suppressor plasmid	Cm	Wagner lab
pMIB5175	pSB890-*invE*	Tet	Wagner lab
pMIB5955	pSB890-SipD-NL	Tet	Wagner lab
pMIB5563	pSB890-SipA-NL	Tet	Wagner lab
pMIB7289	pSB890-InvA$^{HA\text{-}TEV\text{-}FLAG}$	Tet	Wagner lab
pSB3531	pSB890-Δ*invA*	Tet	Wagner lab
pMIB7575	pT10-*invE*	Kan	This study
pMIB7576	pT10-*invE*^{FLAG}	Kan	This study
pMIB7578	pT10^{FLAG}*invE*	Kan	This study
pMIB7579	pT10-*invA*$^{HA\text{-}TEV}$	Kan	This study
pMIB7580	pSB890-Δ*invE*$_{complete}$	Tet	This study
pMIB7721	pSB890-*invE*^{FLAG}	Tet	This study
pMIB7722	pSB890-^{FLAG}*invE*	Tet	This study
pMIB7723	pSB890-*invE*^{StrepTagII}	Tet	This study
pMIB7724	pT10-*invEA*	Kan	This study
pMIB7727	pT10-*invFGE*	Kan	This study
pMIB7728	pT10-invA$_{K368X}$$^{HA\text{-}TEV}$	Kan	This study
pMIB7729	pT10-invA$_{R370X}$$^{HA\text{-}TEV}$	Kan	This study
pMIB7730	pT10-invA$_{F388X}$$^{HA\text{-}TEV}$	Kan	This study
pMIB7781	pT10-invA$_{V420X}$$^{HA\text{-}TEV}$	Kan	This study

pMIB7782	pT10-invA$_{E421X}^{HA\text{-}TEV}$	Kan	This study
pMIB7783	pT10-invA$_{Q422X}^{HA\text{-}TEV}$	Kan	This study
pMIB7784	pT10-invA$_{H449X}^{HA\text{-}TEV}$	Kan	This study
pMIB7785	pT10-invA$_{E469X}^{HA\text{-}TEV}$	Kan	This study
pMIB7786	pT10-invA$_{R522X}^{HA\text{-}TEV}$	Kan	This study
pMIB7787	pT10-invA$_{K603X}^{HA\text{-}TEV}$	Kan	This study
pMIB7788	pT10-invA$_{T608X}^{HA\text{-}TEV}$	Kan	This study
pMIB7789	pT10-invA$_{V648X}^{HA\text{-}TEV}$	Kan	This study
pMIB7790	pSB890-*invE*$_{G225X}$	Tet	This study
pMIB7791	pSB890-*invE*$_{Q326X}$	Tet	This study
pMIB7792	pSB890-*invE*$_{M347X}$	Tet	This study
pMIB7793	pSB890-*invE*$_{I355X}$	Tet	This study
pMIB7794	pSB890-*invE*$_{Y357X}$	Tet	This study
pMIB7797	pT10-*invGE*	Kan	This study
pMIB7914	pT10-*invGE*^{FLAG}	Kan	This study

Table 7 **Primers used in this study** for Gibson cloning and QuikChange site-directed mutagenesis. Primers were synthesized by Eurofins Genomics.

Name	Sequence (5’ to 3’)
Primers used for Gibson cloning	
gib_uni_pT12_f	AGCTTGGCTGTTTTGGCGGATG
gib_uni_pT12_r	GGTGAATTCCTCCTGAATTTC
gib_pT12_invE_f	GGTCGTAATGAAATTCAGGAGGAATTCACCATGATT CCTGGCTCAACCTC
gib_pT12_invE_r	CTCTCATCCGCCAAAACAGCCAAGCTTTAAGACAGC TTTTCAATAGTACGAC
gib_uni_FLAG_f2	TCTAGAGACTACAAAGACCATG
gib_FLAG_invE_r	CACCGTCATGGTCTTTGTAGTCTCTAGAAGACAGCTT TTCAATAGTACGACG
gib_uni_NFLAG_f	GATTACAAGGATGACGATGACAAAGGCAGCATTCCT GGCTCAACCTCCG
gib_uni_NFLAG_r	GCTGCCTTTGTCATCGTCATCCTTGTAATC
gib_uni_invEdown_f	TTTAATATTAACAGGATACCTATAGTGC
gib_uni_invE_r	ATTCCTGGCTCAACCTCCG
gib_invEup_invE_f	GTTTATCTGGATAGAGGTCAGGAGGCAATTAAATGA TTCCTGGCTCA
gib_invEdown_FLAG_r	GAGAAAGCAGCACTATAGGTATCCTGTTAATATTAAA TCATTTGTCATCGTCATCCTTGTAATC

gib_invEup_FLAG_f	GTTTATCTGGATAGAGGTCAGGAGGCAATTAAATGAGTGACTACAAAGACCATGACGG
gib_invEdown_invE_r	GAGAAAGCAGCACTATAGGTATCCTGTTAATATTAAATTAAGACAGCTTTTCAATAGTACGAC
gib_invEdown_StrepTagII_r	GAGAAAGCAGCACTATAGGTATCCTGTTAATATTAAATCATTTTTCGAACTGCGGGTG
gib_uni_pT12b_f	CTAGAGTCGACCTGCAGGCA
InvA_Gc_r	CCAAGCTTGCATGCCTGCAGTTATATTGTTTTTATAACATTCACTGAC
gib_pT12_invF_f	GGTCGTAATGAAATTCAGGAGGAATTCACCATGTCATTTTCTGAAAGCCGACAC
gib_pT12_invG_f	GAAATTCAGGAGGAATTCACCATGAAGACACATATTCTTTTGGCCAG
Primers used for QuikChange site-directed mutagenesis	
QC_invA_dCFLAG_f	GTTATAAAAACAATATCTAGATGATAAGGAAGCTTGGCTGTTTTG
QC_invA_dCFLAG_r	CAAAACAGCCAAGCTTCCTTATCATCTAGATATTGTTTTTATAAC
dinvE_QC_f	GGTCAGGAGGCAATTAAATAATTTAATATTAACAGGATACCTATAGTG
dinvE_QC_r	CACTATAGGTATCCTGTTAATATTAAATTATTTAATTGCCTCCTGACC
invA_K368X_QC_f	GTACCGTTGATATTACTTGTGCCGTAGAGCCGGCGTGAAG
invA_K368X_QC_r	CTTCACGCCGGCTCTACGGCACAAGTAATATCAACGGTAC
invA_R370X_QC_f	GATATTACTTGTGCCGAAGAGCTAGCGTGAAGATCTGGAAAAAGCTC
invA_R370X_QC_r	GAGCTTTTTCCAGATCTTCACGCTAGCTCTTCGGCACAAGTAATATC
invA_F388X_QC_f	AGCGTCTACGTAGTCAGTTCTAGATTGATTATGGCGTGCGC
invA_F388X_QC_r	GCGCACGCCATAATCAATCTAGAACTGACTACGTAGACGCT
invA_V420X_QC_f	GTTGATTAATGAGATCCGTTAGGAACAATTTACGGTCTATTTTGATTTG
invA_V420X_QC_r	CAAATCAAAATAGACCGTAAATTGTTCCTAACGGATCTCATTAATCAAC
invAE421X_QC_f	GAGATCCGTGTTTAGCAATTTACGGTC
invAE421X_QC_r	GACCGTAAATTGCTAAACACGGATCTC
invAQ422X_QC_f	GATCCGTGTTGAATAGTTTACGGTCTATTTTG
invAQ422X_QC_r	CAAAATAGACCGTAAACTATTCAACACGGATC
invAH449X_QC_f	GTATTAATCCAACAATCTAGCAGCAAGGTAGC

invAH449X_QC_r	GCTACCTTGCTGCTAGATTGTTGGATTAATAC
invA_E469X_QC_f	GGGGAGAAACTCCGGTAGCTTGGCTATGTGTTGCG
invA_E469X_QC_r	CGCAACACATAGCCAAGCTACCGGAGTTTCTCCCC
invA_R522X_QC_f	TCCTGATTTACTTAAAGAAGTGCTCTAGCATGCCACG GTACAACGTATATC
invA_R522X_QC_r	GATATACGTTGTACCGTGGCATGCTAGAGCACTTCT TTAAGTAAATCAGGA
invA_K603X_QC_f	GAAGTTGAGGATGTTATTCGCTAGGGGATCCGTCAG AC
invA_K603X_QC_r	GTCTGACGGATCCCCTAGCGAATAACATCCTCAACT TC
invA_T608X_QC_f	GAAGTTGAGGATGTTATTCGC TAG GGGATCCGTCAGAC
invA_T608X_QC_r	CTGAGGAAGGTACTGCCAGACTACTGACGGATCCCT TTGCG
invA_V468X_QC_f	GATCTTGTCCTCCTTACGTCTTAGGATGTCCGTCGAT TTATTAAGAAAATGATTG
invA_V468X_QC_r	CAATCATTTTCTTAATAAATCGACGGACATCCTAAGA CGTAAGGAGGACAAGATC
invE_G255X_QC_f	GAAGAATATTGGCAGGAAGAATTGTTATAGGCGTTA CGTAGTATG
invE_G255X_QC_r	CATACTACGTAACGCCTATAACAATTCTTCCTGCCAA TATTCTTC
invE_Q326X_QC_f	GCGTTACGTAGTATGACCGATTAGGCCTACAAGCAT GAAATGGC
invE_Q326X_QC_r	GCCATTTCATGCTTGTAGGCCTAATCGGTCATACTAC GTAACGC
invE_M347X_QC_f	GTATGACCGATATTGCC TAG AAGCATGAAATGGCAGAAC
invE_M347X_QC_r	GTTCTGCCATTTCATGCTTCTAGGCAATATCGGTCAT AC
invE_I355XX_QC_f	CTGGTGGTACTGGATTTTATTGAG TAG TCGCTATTAACCGATATTGACGC
invE_I355XX_QC_r	GCGTCAATATCGGTTAATAGCGACTACTCAATAAAAT CCAGTACCACCAG
invE_Y357X_QC_f	GAACATGCATCCTTTTTGCAGATATTTTATTAGGTAT GTAAAGCCATACCCTC
invE_Y357X_QC_r	GAGGGTATGGCTTTACATACCTAATAAAATATCTGCA AAAAGGATGCATGTTC

5 Results

5.1 Complementation of *invE* deletions

An important initial step in evaluating potential interaction sites between InvE and InvA by *in vivo* photocrosslinking was establishing plasmid-based complementation of *invE* deletions. This approach should facilitate rapid introduction of amber mutations into various positions of *invE* for subsequent experiments.

5.1.1 Complementation with pT10-*invE*

The chosen plasmid vector was pT10, a low copy number plasmid with an L-rhamnose inducible promotor. *S.* Typhimurium strains with *Δrha*, *ΔaraA-D, ΔinvE,* SipD-NL or *Δrha*, *ΔaraA-D, ΔinvE,* SipA-NL backgrounds served as negative controls. Chromosomal deletion of L-rhamnose and L-arabinose metabolism operons was intended to yield more stable and accurate results and reduce background noise, as these sugars induced the expression of plasmid-encoded genes. Plasmids with an L-arabinose inducible promotor carrying *hilA* to overexpress the SPI-1 T3SS were used for later *in vivo* photocrosslinking experiments.

System functionality was assessed using NanoLuc (NL) luciferase and TCA secretion assays (see Figure 6).

In the NL secretion assay, the Δ*invE* strain exhibited the typical secretion phenotype with almost no discernible secretion of intermediate substrates, exemplified by SipD, and oversecretion of late substrates (SipA) (Figure *6*A+B). This oversecretion was less pronounced than in previous experiments indicating a 10-fold overexpression of SipA (Master Thesis A. Zeitler 2019). However, those studies used an overexpressed SPI-1 T3SS with a *hilA* plasmid, which might account for these differences. The reduced oversecretion led to a smaller dynamic range in the data points, complicating the interpretation of results in this study.

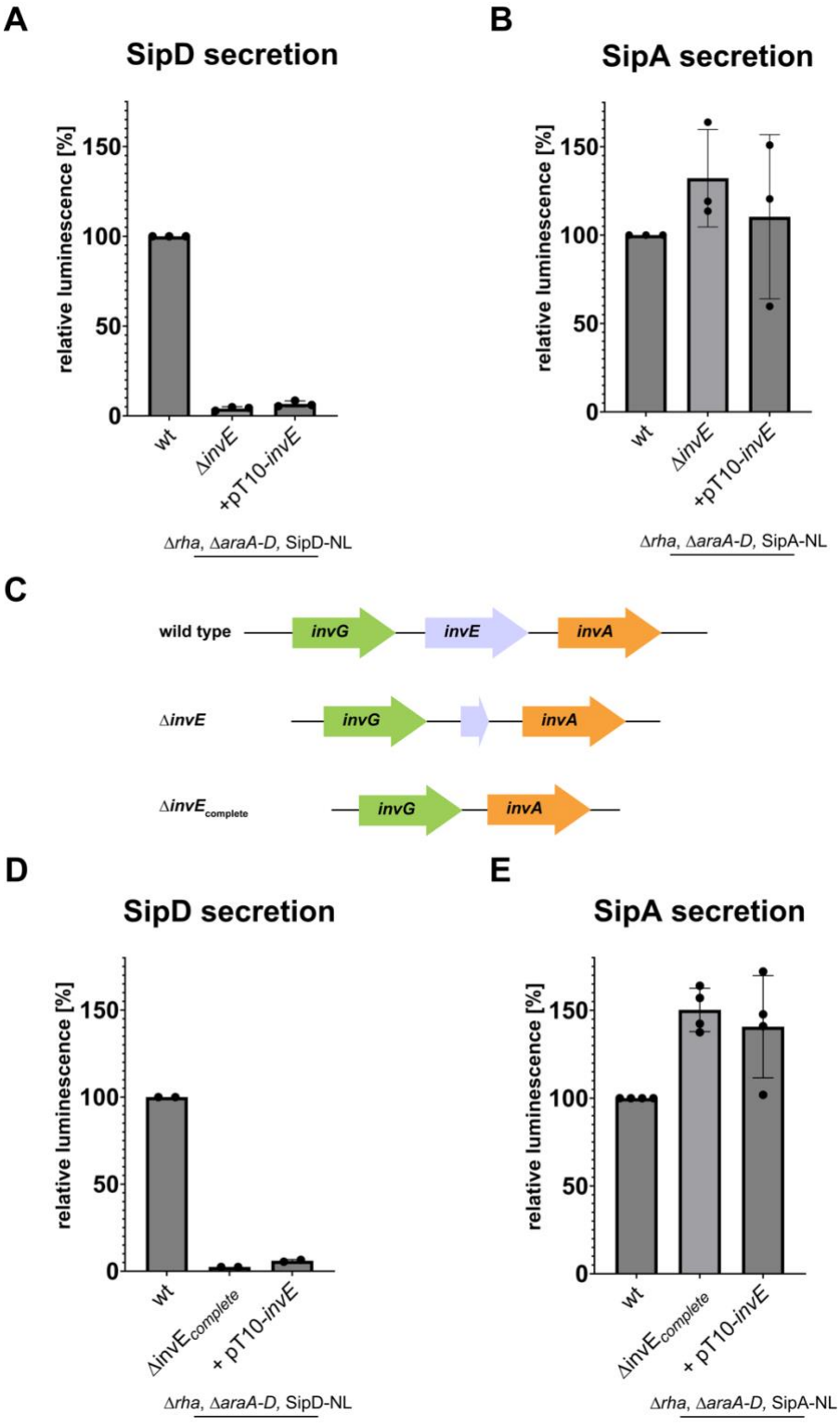

Figure 6. **Plasmid-based complementation of ΔinvE(complete) with pT10-*invE*. (A,B,D,E)** T3SS-mediated secretion of intermediate (A,D) and late (B, E) substrates with a NL secretion assay. pT10-*invE* complementing *S*. Typhimurium Δ*rha*, Δ*araA-D*, Δ*invE* reporter strains were either based on Δ*invE* (deletion with a small part of the gene left) (A,B), or based on Δ*invE*complete (no part of the gene left) (D,E). Plasmid-based gene expression was induced with L-rhamnose. After subtraction of background luminescence, values were normalized to the wild type. Each dot represents a biological replicate, with three technical replicates, respectively. **(C)** cartoon representation of the chromosomal *invGEA* region in wild type and mutant strains.

Notably, the strains that were transformed with pT10-*invE* showed the same secretion phenotype as the negative controls (Figure *6*A+B).

The ∆*invE* strain still contained small portions of the beginning and end of *invE* on the chromosome. I hypothesized that this residual gene fragment might translate into a small peptide that interfered with the function of the plasmid-based InvE protein, possibly by blocking essential binding sites. To rule out this possibility, a new knockout strain deleting the complete *invE* gene was created, resulting in *Δrha*, *ΔaraA-D, ΔinvE*$_{complete}$, SipD-NL or SipA-NL (see Figure *6*C). This strain, transformed with pT10-*invE*, was tested for its respective secretion phenotype but, unfortunately, this plasmid also failed to complement the deletion (Figure *6*D+E).

In summary, the plasmid pT10-*invE* was unable to functionally complement ∆*invE* strains and restore InvE function.

5.1.2 Testing various constructs for complementation

The inability of the plasmid-based *invE* to functionally complement the ∆*invE* deletion highlighted the need to explore underlying molecular mechanisms at play. The failure suggested that the mere presence of the *invE* gene on a plasmid is insufficient for functional complementation. This could stem from a range of issues including transcriptional or translational inefficiencies, or inhibited function of InvE. Considering these possibilities, translational coupling emerged as a potential explanatory factor. Translational coupling is a process where the expression of one gene is dependent on the preceding gene in an operon. This is particularly relevant in operons where coordinated expression is critical for proper function. To investigate this hypothesis, I focused on the potential translational coupling of the *invE* gene with its adjacent chromosomal genes. The genes upstream of *invE* are *invF*, a transcription factor, and *invG*, encoding the secretin, a component of the T3SS's outer ring. Downstream, we find *invA*, which encodes the major export apparatus protein. To investigate the possibility of translational coupling affecting *invE* expression, I constructed and

tested pT10 plasmids harboring either *invFGE* or *invEA* constructs. These plasmids were then tested using secretion assays.

The strain transformed with the pT10-*invEA* plasmid exhibited the same secretion phenotype as the knockout strain for intermediate secretion (Figure 7A). Surprisingly, the pT10-*invFGE* plasmid was able to complement the knockout strain and restored 31.4 (± 11.0) % of secretion of the intermediate substrate SipD (Figure 7B). As previously mentioned, the interpretation of the secretion phenotype of the late substrate SipA is less conclusive (Figure 7C).

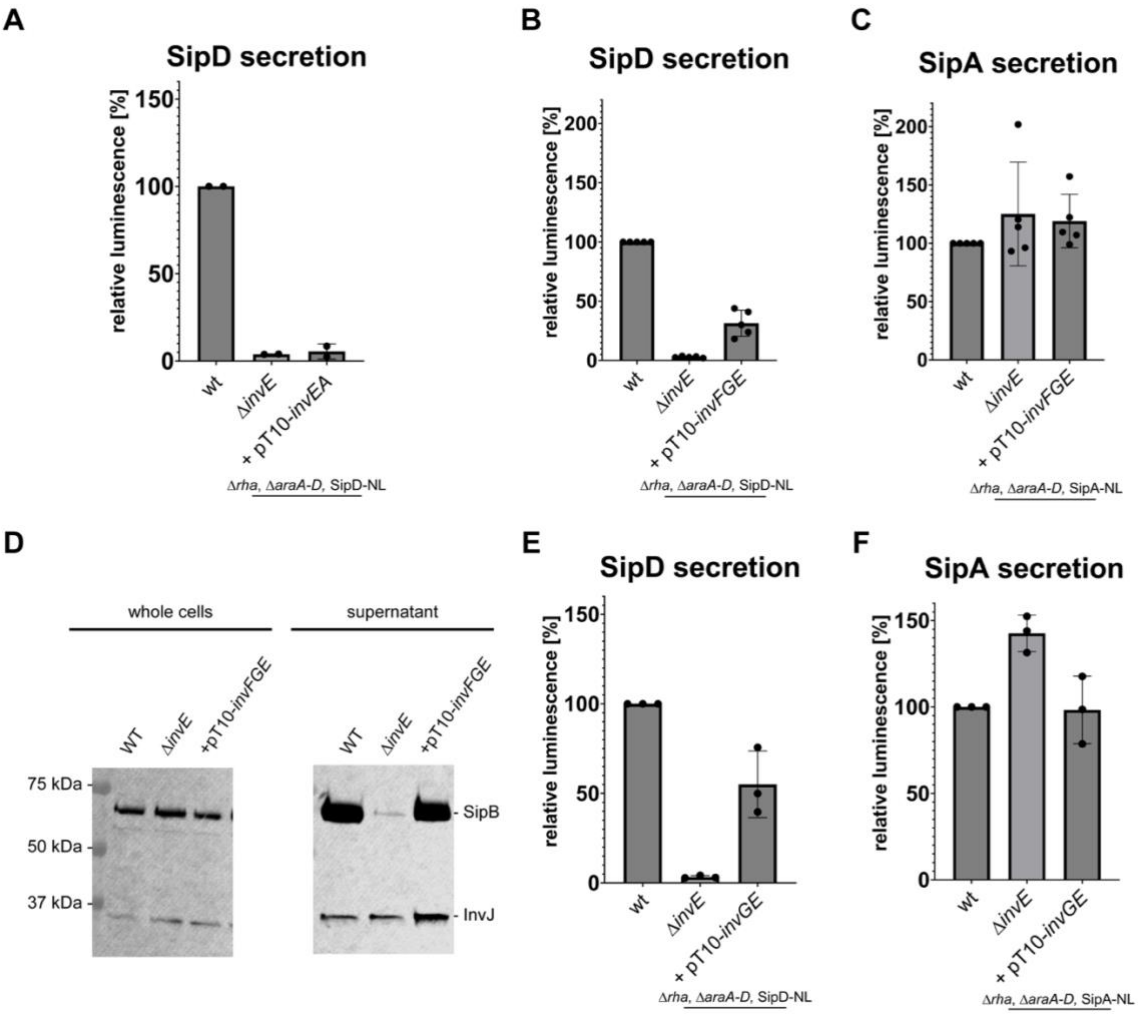

Figure 7. **T3SS-mediated secretion of early (D), intermediate (A,B,D,E) and late (C,F) substrates.** *S*. Typhimurium Δ*rha*, Δ*araA-D*, Δ*invE* was complemented with pT10-*invEA* (A), pT10-*invFGE* (B,C,D), and pT10-*invGE* (E,F). Plasmid-based gene expression was induced with L-rhamnose. **(A-C,E+F)** NL secretion assay. After subtraction of background luminescence, values were normalized to the wild type. Each dot represents a biological replicate, with three technical replicates, respectively. **(D)** TCA secretion assay of complementation with pT10-*invFGE*, one of two biological replicates shown.

Given that 31 % intermediate secretion significantly deviated from the typical Δ*invE* phenotype of 1-3 %, it can be inferred that the plasmid restores some level of wild type secretion. A TCA secretion assay yielded similar results, with the plasmid pT10-*invFGE* restoring intermediate secretion of SipB (Figure 7D).

The plasmid was then shortened to only contain *invGE* for easier handling and to exclude unwanted effects on gene expression regulation by overexpressing transcription factor InvF. The plasmid pT10-*invGE* restored 55.1 (±18.6) % of SipD secretion (Figure 7E+F).

While the restoration of function with the pT10-*inv(F)GE* plasmid was an intriguing development, it also raised a new question: Why did extending the sequence upstream of *invE* improve its expression and function? The mRNA structured might be influenced by the pT10 vector design, which in turn might affect the translation initiation of invE. This observation led me to examine the mRNA secondary structure of the different constructs. I used RNAfold based on the ViennaRNA Package (Version 2.4.18) to predict the mRNA secondary structures of the pT10-*invE* plasmid and the chromosomal *invGE* region.

For the plasmid, the promoter region of the pT10 vector appeared to form a strong stem-loop structure with the first 50 base pairs of invE, potentially preventing the initiation of translation of *invE* (Figure 8A). Conversely, the corresponding chromosomal region, where *invG* and *invE* overlap, resulted in a much weaker stem-loop formation, suggesting less interference with translation (Figure 8B).

Consequently, while the pT10-*invE* accidentally created a self-repressing mRNA, a plasmid harboring the same upstream region of *invE* as on the chromosome is likely to result in de-repression of *invE* translation. This provided a logical explanation for the above results and serves as a fresh affirmation of the importance of mRNA secondary structures in protein biosynthesis.

Preliminary data suggested that a silent point mutation at the beginning of *invE* could destabilize the stem-loop structure and ensure de-repression of

translation of plasmid-based *invE*. However, such a construct will have to be the focus of future research efforts.

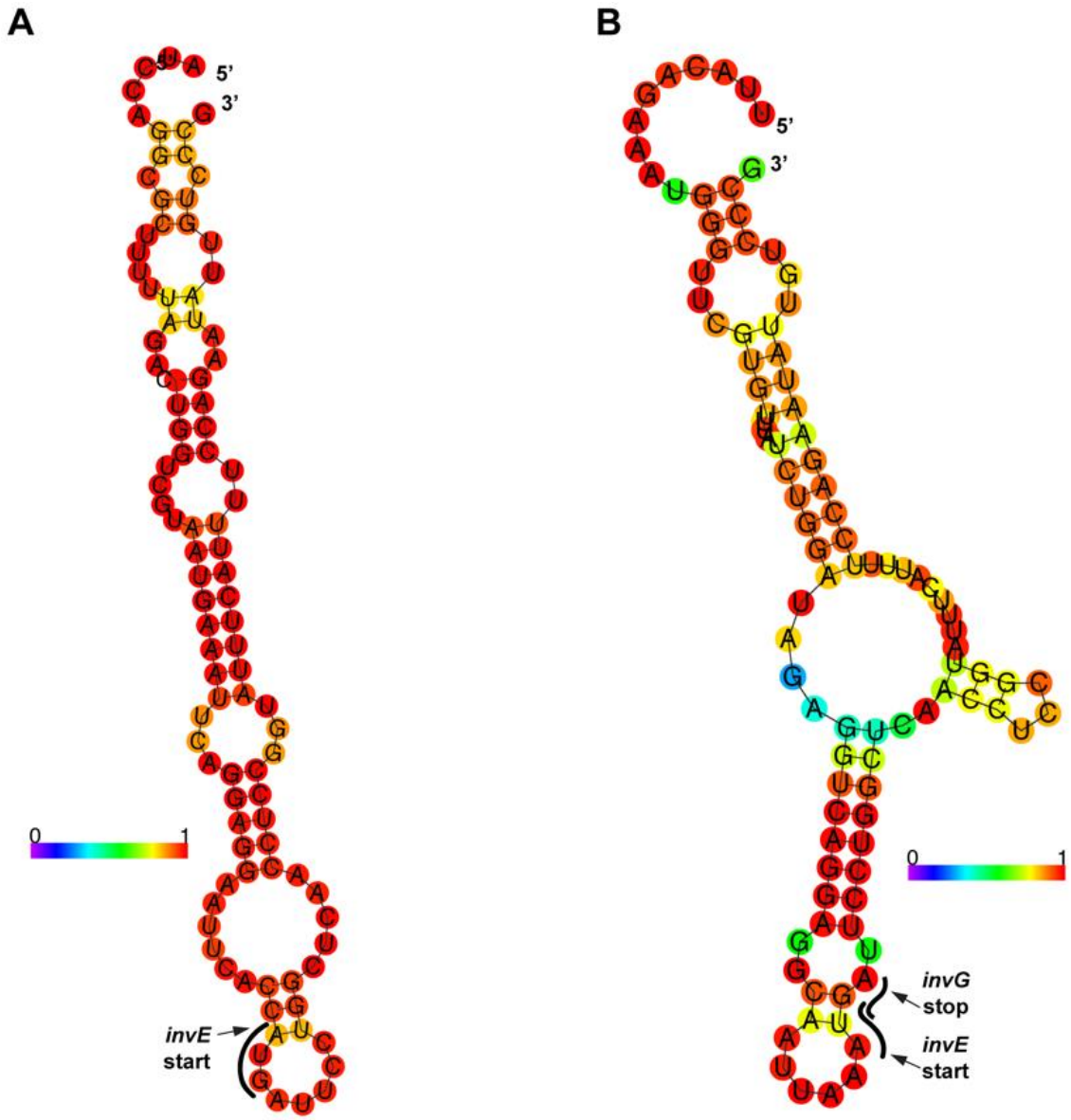

Figure 8. **RNAfold prediction of the mRNA of pT10-*invE* (A), (B) *invGE*, and pT10-^{FLAG}*invE* (C).** Color coding represents base-pair probabilities. **(A)** mRNA prediction of the 30 base pairs of the pT10 promotor region and the first 50 base pairs of *invE*; **(B)** mRNA prediction of the last 50 base pairs of *invG* and the first 50 base pairs of *invE*; **(C)** same area as in (A), but with the additional 72 base pairs of the FLAG-tag.

5.2 Development of a functional epitope tagged InvE

In pursuit of facilitating *in vivo* photo-crosslinking experiments, the development of a functionally epitope-tagged InvE was crucial for immunodetection.

Initial attempts focused on a plasmid-based system with InvE tagged at both the N- and C-termini with FLAG tags. These constructs, pT10-^{FLAG}*invE* and pT10-*invE*^{FLAG}, were assessed through NL and TCA secretion assays (Figure 9A-C). These trials did not result in functional complementation, as the strains with the tagged plasmids exhibited secretion phenotypes akin to the Δ*invE* deletion, analogically to the results detailed in section 5.1.1.

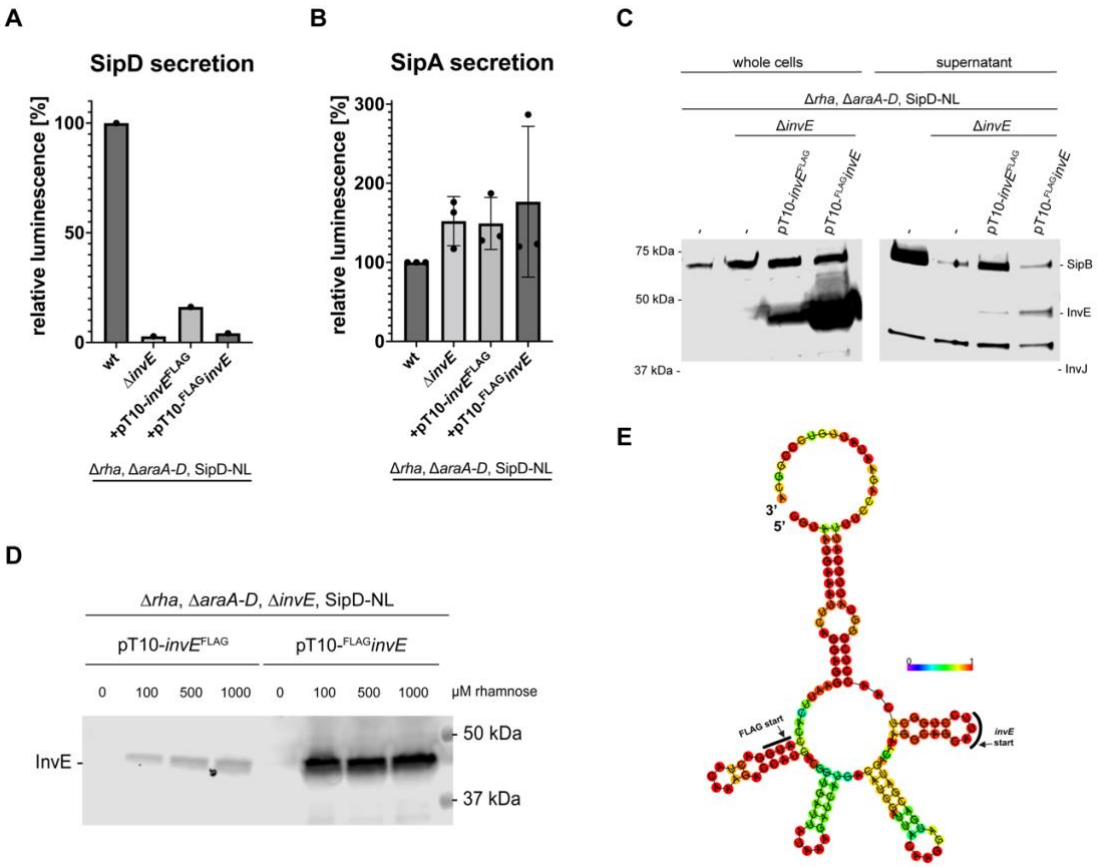

Figure 9 **Functional analysis of S. Typhimurium Δ*rha*, Δ*araA-D*, Δ*invE*, SipD-NL or SipA-NL with pT10-*invE*^{FLAG} and pT10-^{FLAG}*invE*. (A,B)** NL secretion assay of intermediate (A) and late (B) substrates. After subtraction of background luminescence, values were normalized to the wild type. Each dot represents a biological replicate, with three technical replicates, respectively; **(C)** TCA secretion assay of early and intermediate substrates, one of two biological replicates shown; **(D)** Whole cell samples were analyzed by SDS-PAGE and Western blot. Samples were induced with varying amounts of rhamnose at the start of the culture. Immunodetection was performed with antibodies against the FLAG-tag; **(E)** RNAfold prediction of the mRNA pT10-^{FLAG}*invE* with 30 base pairs of the pT10 promotor region, 72 base pairs of the FLAG-tag and the first 50 base pairs of *invE*. Color coding represents base-pair probabilities.

In the TCA assays, the plasmid pT10-*invE*^{FLAG} appeared to restore SipB secretion, a result consistent across multiple replicates. However, the reliability of this observation must be treated with caution due to contradictory results in one replicate, where SipB secretion was also seen in the Δ*invE* negative control (Figure 9C).

Additionally, while InvE was detectable in the supernatant, suggesting secretion of the gatekeeper protein, the low quantity relative to whole cells raised questions about physiological relevance. It was considered that these faint bands might represent InvE from lysed cells rather than authentic secretion (discussion in Section 6.3).

To test translational efficiency and protein stability in a plasmid-based setting, epitope-tagged InvE was also evaluated through SDS-PAGE and Western blot analysis, revealing higher accumulation levels for ^{FLAG}InvE compared to InvE^{FLAG} (Figure 9D).

This led to an investigation into the mRNA structure of pT10-^{FLAG}*invE* using RNAfold, which indicated a shorter stem-loop structure than pT10-*invE* potentially explaining the higher levels of accumulation (Figure 9E).

Given the unsuccessful plasmid-based complementation at that stage, functionality of tagged InvE was evaluated on the chromosome. I attempted N- and C-terminal tagging of chromosomal InvE with a FLAG-tag and a Strep-tag II but was unsuccessful in creating an N-terminal Strep-tag II.

The various constructs were assessed using NL assays for intermediate and late secretion, compared to wild type *invE*. It was found that C-terminal tagging of InvE did not interfere with its function, as evidenced by secretion phenotypes matching those of the wild type for both FLAG-tag and Strep-tag II constructs (Figure *10*A+B). Contrastingly, the N-terminally FLAG-tagged InvE strain displayed a phenotype like a Δ*invE* strain, characterized by abolished intermediate substrate secretion (SipD) and slight oversecretion of late substrate SipA. This suggests that while C-terminal tagging is non-disruptive, N-terminal tagging impairs InvE function.

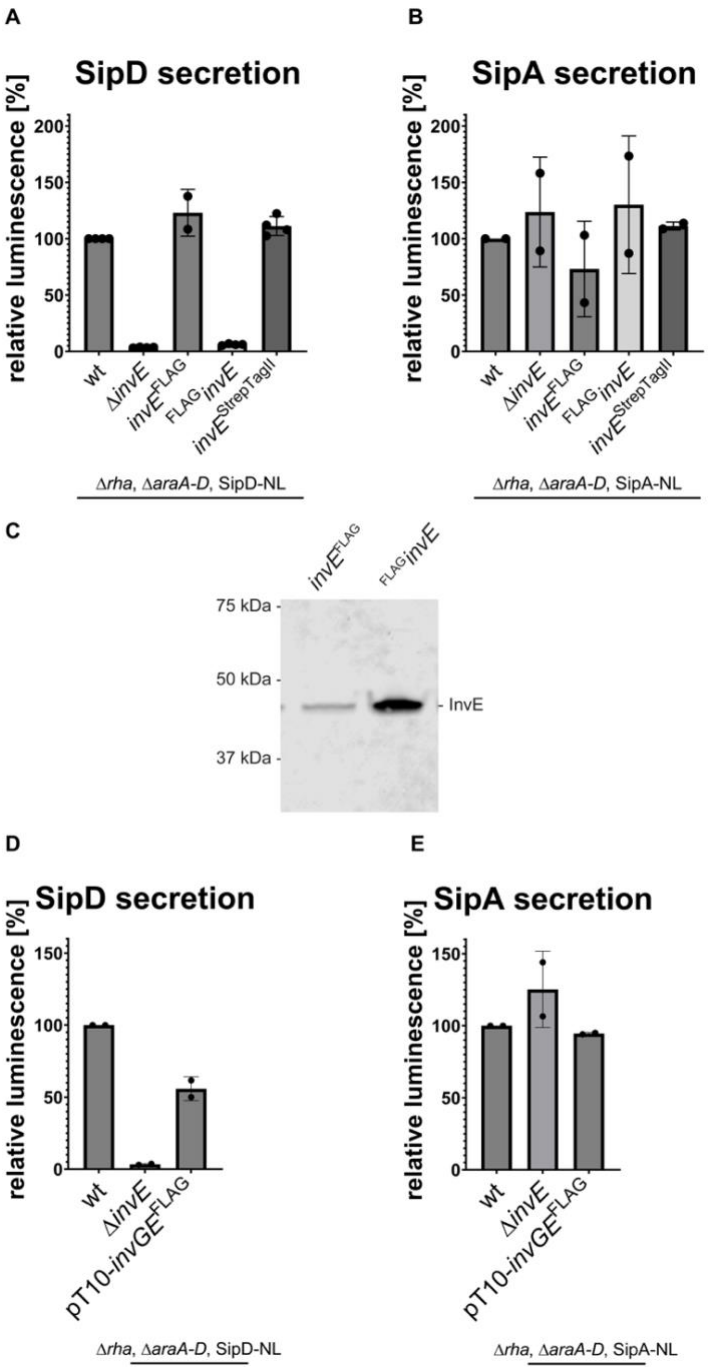

Figure 10. **Development of epitope-tagged *invE*. (A,B)** T3SS-mediated secretion of *S.* Typhimurium Δ*rha*, Δ*araA-D* with chromosomal epitope-tagged *invE*. NL assay was performed for intermediate (A) and late (B) substrates. After subtraction of background luminescence, values were normalized to the wild type. Each dot represents a biological replicate, with three technical replicates, respectively. **(C)** SDS-PAGE and Western blot of whole cells from S. Typhimurium Δ*rha*, Δ*araA-D*, SipD-NL with *invE*^{FLAG} or ^{FLAG}*invE*. **(D, E)** T3SS-mediated secretion of *S.* Typhimurium Δ*rha*, Δ*araA-D* complemented with pT10-inv*GE*^{FLAG}. Plasmid-based gene expression was induced with L-rhamnose. After subtraction of background luminescence, values were normalized to the wild type. Each dot represents a biological replicate, with three technical replicates, respectively.

Further assessment of epitope-tagging was conducted through SDS-PAGE and Western blot analyses. These tests confirmed the presence of both FLAG-tagged constructs, with notably stronger signals for the N-terminally tagged InvE (Figure *10*C). The C-terminal Strep-tag II, however, was not detectable.

In summary, introducing a FLAG-tag at the C-terminus of InvE resulted in a functional and detectable InvE mutant, suitbale for further experiments.

Building on the experimental insights from the previous chapters – specifically, that plasmid-based complementation of Δ*invE* worked with pT10-*invGE*, and that C-terminal FLAG-tagging resulted in functional InvE – I then tested the complementation of Δ*invE* with pT10-*invGE*^{FLAG} using a NL secretion assay. This was to ensure that the FLAG-tag did not impede InvE function in a plasmid-based context. The plasmid restored SipD secretion to 55.9 (±8.2) % of the wild type level (see Figure 10D+E). Therefore, pT10-*invGE*^{FLAG} is suitable for further experimental use.

5.3 Testing multiple positions in InvE for interaction with InvA

Interactions between the gatekeeper InvE and the major export apparatus protein InvA were investigated by *in vivo* photo-crosslinking. Various potential interactions sites on InvE and InvA were tested using two approaches. In the first approach, amber mutations were introduced into chromosomal *invE*, and the chromosomal *invA* contained both HA- and FLAG-tags (described in this section 5.3). In the second approach, amber mutations were introduced into plasmid-based *invA*. For this, dual epitope-tagging was employed, wherein chromosomal *invE* contained an FLAG-epitope-tag, and *invA* on the plasmid carried an HA-epitope-tag (detailed in sections 5.4 and 5.5). These distinct tagging strategies facilitated a clear identification and analysis of the protein-protein interactions between InvE and InvA.

For the first exmperiments, *S.* Typhimurium Δ*rha*, Δ*araA-D*, *invA*$^{HA\text{-}TEV\text{-}FLAG}$, *invE*$_{QC}$, SipD-NL strains were used due to time constrains, given that the plasmid-based complementation of Δ*invE* had not been established at this

stage. Amber mutations for the amino acid *para*-benzoyl-L-phenylalanine (*p*Bpa) were introduced into the chromosomal *invE*. Photo-crosslinking was induced by UV illumination, and crude membrane samples were subjected to SDS-PAGE and Western blot, followed by immunodetection against the FLAG-tag in InvA. Additionally, a NL secretion assay was performed to evaluate possible functional deficits of the SPI-1 T3SS caused by the mutations in InvE (see Figure 11).

The intermediate secretion analysis indicated that the point mutations did not completely abolish the secretion function of the SPI-1 T3SS (Figure *11*A). Positions Q326X, M347X, I355X, and Y357X showed SipD secretion levels between 99 % to 132 %, compared to the positive control, wild type InvE. Notably, SipD secretion at position G255X decreased to 61 % of the wild type. However, due to the sensitivity of the NL secretion assay, this reduction could be attributed to various factors, including technical inaccuracies, and would require repetition of the experiment for confirmation. Remarkably, only position M347X showed diminished late secretion of SipA at 80 % compared to the wild type (Figure *11*B). Position G255X had the second-lowest at 139 % secretion compared to the wild type. The other positions, namely Q326X, I355X, and Y357X, oversecreted the late substrate SipA at 215 % to 296 %. None of the positions completely abolished the secretion of intermediate effectors, nor did they resemble a Δ*invE* secretion phenotype, which would be indicative of mutations disrupting InvE function. Consequently, I conclude that the amber mutations in InvE do not significantly compromise the protein's function.

With the epitope-tag in InvA, interactions between InvA and InvE could be detected, but interactions between InvE and other proteins could not. InvA has a molecular weight of 76.1 kDa. Therefore, any upshift in protein size observed in the UV (+) samples, compared to the UV (-) samples and the $InvE_{noQC}$ control, would indicate that InvE crosslinked to InvA at the mutated position. However, no detectable crosslink was observed at any of the tested positions (Figure 11C).

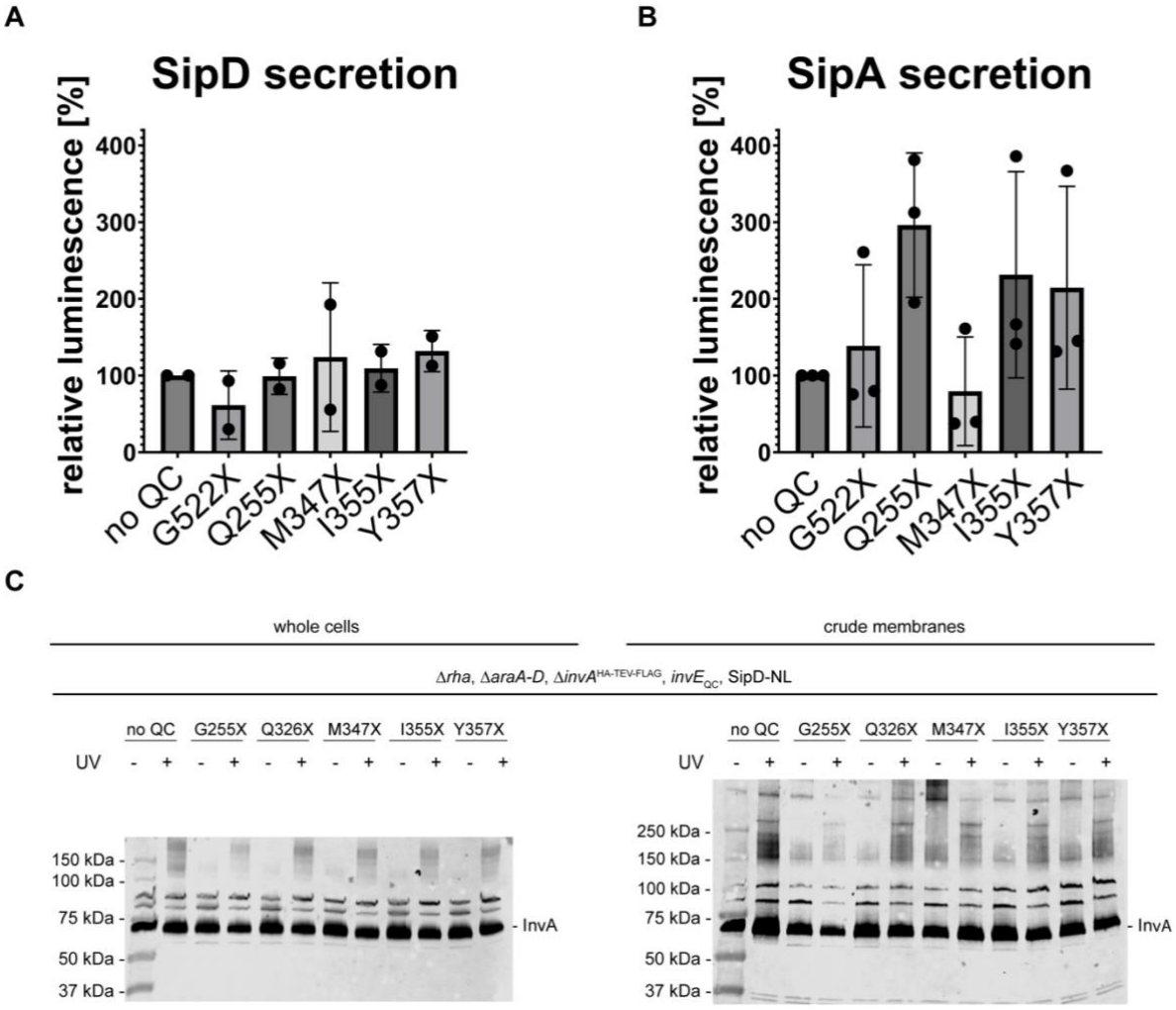

Figure 11 **Crosslinking multiple positions in InvE for possible protein-protein interactions**
(A,B) T3SS-mediated secretion of intermediate (A) and late (B) substrates of *S.* Typhimurium Δ*rha*, Δ*araA-D*, Δ*invA*$^{HA\text{-}TEV\text{-}FLAG}$, *invE*$_{QC}$. After subtraction of background luminescence, values were normalized to the wild type. Each dot represents one biological replicate, with three technical replicates, respectively.
(C) Protein-protein interactions of InvA and InvE were tested by *in vivo* photo-crosslinking with *p*Bpa mutations (X) in G255, Q326, M347, I355, and Y357 of *invE*. Samples were treated without (-) or with (+) UV to induce crosslinking, and then subjected to SDS-PAGE and Western blot. For immunodetection, antibodies against the HA-tag were used.

5.4 Effect of various amber mutations on InvA function

In this second approach, *S.* Typhimurium Δ*rha*, Δ*araA-D*, *invE*^{FLAG}, Δ*invA* strains were transformed with pT10-*invA*$_{QC}^{HA\text{-}TEV}$ (overview of tested positions mapped on InvA in Figure 12A). Using both FLAG-tags in InvE and HA-tags in InvA allowed differentiation between InvA's specific crosslinks with InvE and its crosslinks with other proteins.

It was previously established that the plasmid pT10-*invA*$^{HA\text{-}TEV}$ could functionally complement Δ*invA* strains. In this project, control strains with the non-mutated plasmid-based InvA exhibited at least 36 % (SipD) of the wild type secretion levels (Figure 12B+C).

Functional complementation of all positions was tested using a NL assay (Figure 12D+E). Since InvA is crucial for the T3SS, its deletion results in a completely abolished secretion of intermediate and late substrates, making Δ*invA* a useful negative control. Four positions (V420, E421, R522, and K603) displayed virtually no intermediate secretion and severely reduced late secretion levels, with 1.4 – 2.4 % SipD secretion compared to the wild type *invA*. These numbers are similar to the Δ*invA* reduction of SipD secretion (1.8 %). Additionally, the late secretion at these positions was not significantly different from that in Δ*invA*. Two other positions, Q422 and T608, showed mixed results: Q422 had a similar SipD secretion pattern to Δ*invA* (3.8 % compared to wild type) but secreted 16.7 (± 6.2) % of SipA, significantly different from Δ*invA*. T608 exhibited a varied secretion pattern, with intermediate secretion at 10.2 (± 8.3) % and late secretion at 53.3 (± 61.2) %, the latter being statistically indistinguishable from Δ*invA*. This variability might be due to biological factors or stochastic processes during InvA folding, either resulting in a functional or dysfunctional export apparatus protein.

In summary, positions V420, E421, R522, and K603 appeared to critically alter InvA, resulting in almost nonexistent intermediate and late secretion. The results for Q422 were ambiguous but suggested substantial reduction in secretion. Position T608 showed high variability, with secretion outcomes statistically similar to Δ*invA* for late substrates. All these positions failed to demonstrate the expected phenotype of unaltered and fully functional InvA.

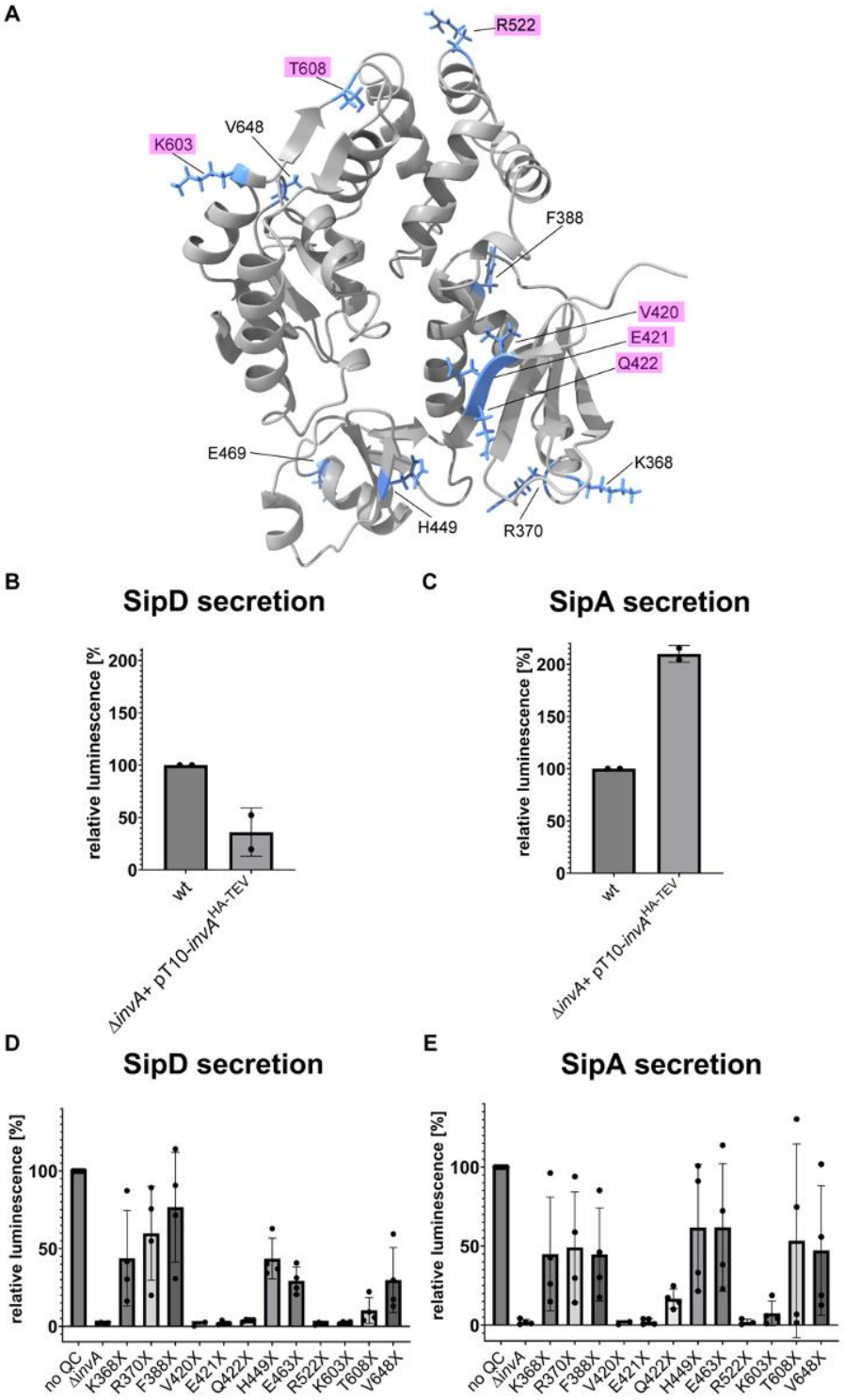

Figure 12 **T3SS-mediated secretion of *S. Typhimurium* Δ*rha,* Δ*araA-D, invE*^{FLAG}**, Δ*invA,* SipD-NL/ SipA-NL complemented with various *pT10-invA*$_{QC}$$^{HA\text{-}TEV}$ constructs**. NL Assay was performed for intermediate (B,D) and late (C,E) substrates. Plasmid-based genes were expressed upon induction with L-rhamnose. After subtraction of background luminescence, values were normalized to the wild type. Each dot represents one biological replicate, with three technical replicates, respectively. **(A)** Protein structure of InvA (predicted by AlphaFold) with positions of amber mutations (highlighted pink: deviant secretion pattern, compared to expectation for intact InvA). **(B,C)** Complementation of Δ*invA* with pT10-*invA*$^{HA\text{-}TEV}$. Values were normalized to the wild type. **(D,E)** Various point mutations in *invA* affect intermediate and late secretion differently. Values were normalized to *S. Typhimurium* Δ*rha,* Δ*araA-D, invE*^{FLAG}*,* Δ*invA, pT10-invA*$^{HA\text{-}TEV}$.

Other positions (K368, R370, F388, H449, E469, and V648) consistently showed higher levels of both intermediate and late secretion, ranging from 29 - 77 % (SipD), or 17 - 62 % (SipA), which was significantly different from the negative control. The high variance in the data points might be due to biological variability and the assay's sensitivity to slight procedural variations. Overall, these positions did not appear to inhibit InvA's function in a way that significantly alters T3SS-dependent intermediate and late secretion. TCA secretion assays confirmed these results (data not shown).
Additionally, InvA protein expression and assembly were assessed using SDS and BN PAGE (Figure 13). The SDS PAGE expression pattern of InvA correlated with the functional pattern observed in the secretion assays: Positions V420, E421, R522, and K603 had fainter bands compared to the wild type. Q422, which showed abolished intermediate and sparse late secretion, exhibited a stronger band. For T608, the band intensity varied across replicates. Despite reduced intensity compared to the wild type and other amber mutations, some residual protein presence was noted, stronger than the Δ*invA* negative control. Additional bands observed in SDS PAGE for Q422, H449, E469, and R522, likely represented truncated InvA proteins, resulting from the amber mutations.

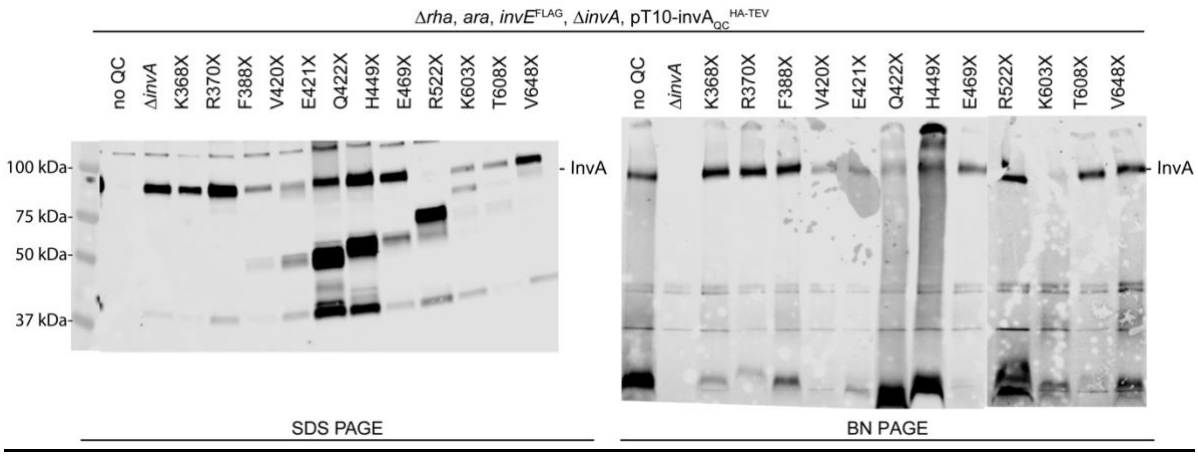

Figure 13 **Protein expression and assembly of InvA carrying various amber mutations**. *S.* Typhimurium Δ*rha,* Δ*araA-D*, *invE*^{FLAG}, Δ*invA* was complemented with pT10-invA$_{QC}$$^{HA-TEV}$. Crude membrane samples were subjected to SDS PAGE and BN PAGE, followed by immunodetection with antibodies against the HA-tag. Shown is one of two biological replicates.

BN PAGE results mirrored these findings: Reduced, but visible signals for V420, E421, Q422, and K603, with T608 comparable to other functional positions. For both replicates, R522 showed a relatively strong signal. This signal most likely represented the truncated InvA which was seen on SDS Page and should have a molecular weight of 59.73 kDa.

Therefore, the impact of these point mutations on secretion assay performance could be partially explained by their effect on protein expression and assembly. The mutations on V420, E421, Q422, R522, and K603 reduced protein expression and assembly but did not eliminate them. T608 showed ambiguous results.

5.5 Testing multiple positions in InvA for protein-protein interactions

All tested positions were then evaluated for protein-protein interactions through *in vivo* photo-crosslinking.

S. Typhimurium Δ*rha*, Δ*araA-D*, *invE*^{FLAG}, Δ*invA* strains carrying pT10-*invA*$_{QC}^{HA-TEV}$ were subjected to UV irradiation. Both whole cell (data not shown) and crude membrane samples were analyzed using SDS-PAGE. The membranes were initially probed with antibodies against the FLAG-tag in InvE, followed by immunodetection of the HA-tag to differentiate crosslinks between InvA and InvE from interactions of InvA with other proteins (Figure 14).

Interestingly, none of the positions demonstrated crosslinks of InvA to InvE. However, crosslinking adducts were detectable at approximately 100 kDa for positions Q422, H449, E469, R522, K603, and V648. Notably, position F388 exhibited two strong crosslink signals at approximately 150 kDa and 200 kDa. Additionally, E469 showed a crosslink at approximately 150 kDa.

In summary, positions F388 and E469 induced crosslinks at 150 and 200 kDa. Moreover, crosslinking adducts at approximately 100 kDa were observed for several positions in InvA. However, no direct interactions between InvA and InvE were detected.

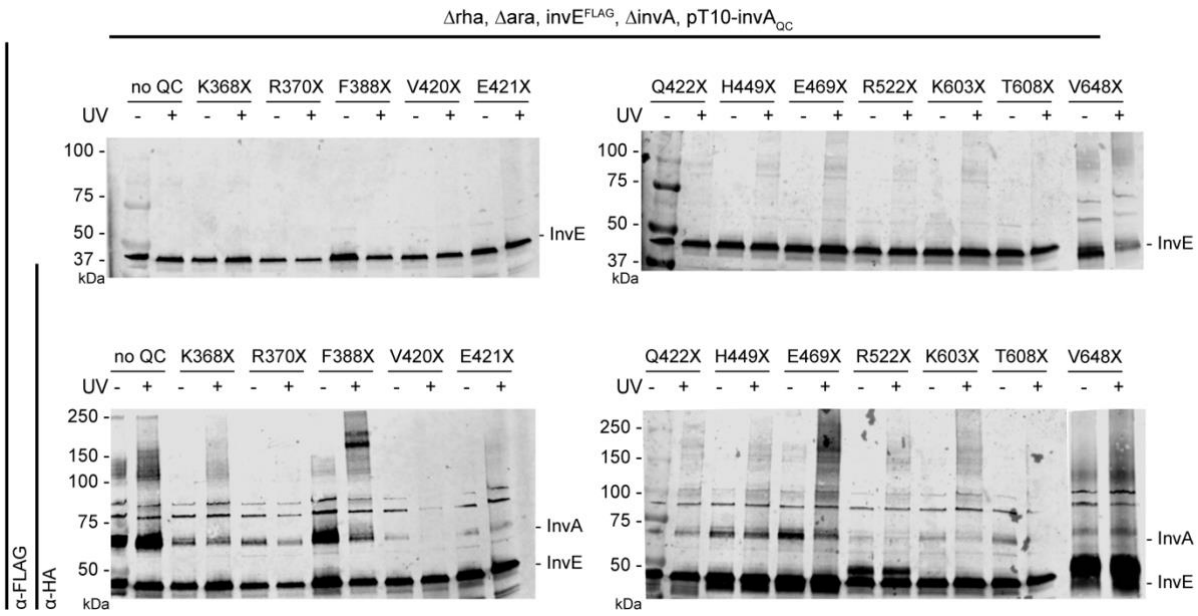

Figure 14 **Analysis of possible protein-protein interactions of multiple positions in InvA by *in vivo* photo-crosslinking.** Samples of *S. Typhimurium* Δ*rha,* Δ*araA-D, invE*^{FLAG}, Δ*invA, pT10-invA*$_{QC}$$^{HA\text{-}TEV}$ were treated with (+) or without (-) UV to induce crosslinking. Crude membrane samples were subjected to SDS PAGE and Western Blot. For immunodetection, antibodies against FLAG-Tag (top) were used, followed by immunodetection against the HA-Tag (bottom). This is one of four replicates.

Given that InvA has a molecular mass of 76.1 kDa and is known to form a nonameric ring, the crosslinks observed at approximately 150 kDa for F388 and E469 suggest interactions between two InvA protomers. Potential interaction partners of InvA could also include components of the needle complex, such as the inner membrane (IM) ring protein PrgK, with a molecular mass of 28.2 kDa, and proteins that belong to the minor export apparatus, like SpaQ (36.0 kDa) and N-terminal fragment of SpaS (28.7 kDa). These associations are inferred based on functional context and the structural proximity observed in cyro-electron tomograms (Kuhlen et al., 2018). However, direct evidence for interactions between these proteins and InvA has not yet been established. Additionally, a crosslink for F388 at approximately 175 kDa was detected. The specific interaction of InvA with other proteins at this molecular weight is yet to be determined. Further experiments will be necessary to elucidate this aspect.

6 Discussion

Substrate specificity switching is a critical component in maintaining the secretion hierarchy in T3S. The mechanisms driving the second switch between the different classes of substrates are largely unclear. However, the interaction between the major export apparatus protein SctV and the gatekeeper protein SctW is believed to be crucial for the switch between intermediate and late secretion. To investigate a potential interaction between InvA (SctV homolog) and InvE (SctW homolog) in the SPI-1 T3SS of *S.* Typhimurium, *in vivo* photocrosslinking experiments were conducted, focusing on positions identified in previous studies (Portaliou *et al.*, 2017; Xing *et al.*, 2018; Yu *et al.*, 2018).

6.1 Quantification of the Δ*invE* secretion phenotype

Deletion of the *invE* gene results in the previously described abolishment of secretion of intermediate substrates, and a slight increase in late secretion, measured at 135 ± 28 % (n=17, from this thesis' experiments). These findings align with prior studies and highlight InvE's central role in the second switch (Kubori and Galán, 2002; Yu *et al.*, 2010). While many studies have described oversecretion of late substrates, quantification of this effect has been limited. One study employing the same NanoLuc luciferase-based T3SS secretion and injection assay as this current study reported approximately a 2-fold increase in the secretion of the effector molecule SipA (Westerhausen *et al.*, 2020). This study corroborates oversecretion in this range and expands these finding with additional experiments in varied contexts. However, the results on late secretion exhibited considerable variance, potentially due to the high sensitivity of the assay, which could capture minor changes in experimental execution and natural biological variability.

The results from this study are consistent with the previous data on the secretion phenotype of Δ*invE* mutant strains and underscore the importance of InvE in controlling intermediate and late secretion. The implementation of the

NL assay in this study provides a precise quantification of these processes. Further experiments could delve deeper into the molecular mechanisms that establish the T3S hierarchy and the connection between SctW function and the first switch. Investigating combined mutants, such as Δ*invE* with Δ*sctP* (the ruler protein) or a mutation inhibiting SctU autocleavage ($SctU_{N258}$), could offer further insights. Since SctP and SctU autocleavage are key in substrate specificity switching and host cell sensing, analyzing these combined mutants' secretion phenotypes could enhance understanding of the switching requirements, the roles of various regulators, and the hierarchy among them.

6.2 Plasmid-based *invE*

In this study, pT10-*invE* plasmids were unable to complement *invE* knockout mutants, in contrast to pT10-*invGE* plasmids. Several factors could potentially explain the failure of plasmid-based complementation: reduced *invE* transcription and translation, inhibited InvE function, or rapid InvE degradation in the cytoplasm. Interestingly, samples with pT10-*invE* carrying C- or N-terminal FLAG-tags, when subjected to SDS-PAGE and Western blot, displayed differences in signal strength. The protein was detectable in both cases, suggesting some level of transcription, translation, and stability. Notably, the ^{FLAG}InvE construct showed higher accumulation, which might be explained by the mRNA structure of this construct compared to pT10-*invE*^{FLAG}: The N-terminal epitope-tag in front of *invE* results in a shorter stem-loop structure in the mRNA secondary structure compared to pT10-*invE*, which has a stronger stem-loop. These findings imply that pT10-*invE* created an unfavorable mRNA secondary structure, likely reducing translational efficiency and hence its ability to complement Δ*invE* strains. Further investigation into protein stability could be conducted with pulse-chase analysis.

Previous studies have achieved plasmid-based complementation with using *invE* alone as an insert, employing different vectors like the suicide plasmid pSB360, and pBAD24 (Kaniga, Bossio and Galán, 1994; Kubori and Galán, 2002; Kim *et al.*, 2013). However, using the pT10-*invGE* plasmid is not optimal

due to its large size (the insert is about 2.8 kbp long) and the unnecessary overexpression of *invG*. Although InvG, the SctC homolog, is part of the injectisome's base and its overexpression should not directly interfere with T3S regulation, it is still preferable to avoid unnecessary overexpression. Assembly and secretion experiments did not show notable differences when using pT10-*invGE* compared to the wild type. In conclusion, mRNA structures should be carefully considered in cloning designs, and the pT10-*invGE* plasmid can be utilized for future studies to functionally complement Δ*invE* strains. Additionally, a shorter and more efficient plasmid could be developed by introducing a silent mutation at the beginning of invE to create a construct with a more favorable mRNA structure. Initial experiments in this direction have shown promise (data not shown).

6.3 C-terminal and N-terminal epitope-tagging of InvE

In this study, only C-terminal tagging resulted in a functional InvE, while N-terminal tagging exhibited a Δ*invE* secretion phenotype. This indicates a potential requirement for an unobstructed N-terminus for InvE's role, aligning with previous research that has successfully implemented C-terminal tags (Kim *et al.*, 2013). However, it's interesting to note that in one study, GST was fused to the N-terminus of InvE, and this construct successfully restored ∆*invE* function in terms of intermediate secretion (SipB, the SctE homolog, and SipC, the SctB homolog) and cell invasion (Kubori and Galán, 2002), challenging bioinformatics predicitions of an N-terminal secretion signal of InvE (Deng *et al.*, 2005b; Samudrala, Heffron and McDermott, 2009). In another study, proteins fused to N-terminal fragments of SepL in *E.* coli were secreted and translocated (Younis *et al.*, 2010), with speculations that the C-terminus of SepL might prevent secretion and translocation until the right requirements lead to conformational changes that disrupt the C-terminus.

Interestingly, this thesis's classical secretion assays detected both C- and N-terminally FLAG-tagged InvE in the supernatant, albeit at significantly lower levels than in whole cells. This casts doubt on whether such levels of InvE in the

supernatant are physiologically meaningful or merely the result of cell lysis contamination. The strains evaluated did not interact with host cells, which could argue against the physiological necessity of InvE secretion at this infection stage.

A more recent study also noted that an N-terminal FLAG-tag results in a Δ*invE* phenotype, suggesting that any interference at the N-terminus, including tagging, can disrupt function as effectively as deleting the putative secretion signal. This impairment was hypothesized not to stem from interactions with intermediate substrates but possibly from altering InvE's structural conformation or its interactions with other proteins. It was proposed that InvE's N-terminus may undergo proteolytic processing post host-cell sensing, which could lead to effector secretion (Kim *et al.*, 2013).

The physiological significance of the gatekeeper's N-terminal secretion signal remains enigmatic, even though both the N- and C-terminal regions of SctW are essential for intermediate secretion (Kim *et al.*, 2013). The discrepancy between the functional impact of N-terminal FLAG- and GST-tags remains unresolved and may relate to differences in experimental conditions, such as the plasmid vectors used.

Although the exact reasons for the differential effects of N-terminal tagging are elusive, it can be said that C-terminal tagging does not compromise InvE's functionality, and therefore, is suitable for subsequent studies. Prospectively, the development of InvE-specific antibodies would provide a more straightforward and versatile method for detecting InvE across various experimental contexts.

6.4 Functional domains in InvA

In this study, twelve positions in InvA were evaluated for a predicted interaction with InvE. Of these, V420, E421, Q422, R522, and K603 lead to a severe impairment in InvA function, as indicated by reduced protein expression, assembly, and a Δ*invA* secretion phenotype. Position T608 resulted in highly

variable data points with a high standard deviation, statistically indistinguishable from the Δ*invA* phenotype. The other positions did not significantly alter InvA function. For some positions, crosslinking adducts were detected at approximately 100 kDa. Specifically, positions F388 exhibited two strong crosslinks at approximately 150 kDa and 200 kDa, and E469 at approximately 150 kDa. To better understand these results, the positions were mapped on the nonameric structure of InvA, predicted by AlphaFold, Alphabet's and Google's DeepMind AI protein structure prediction program (see Figure 15).

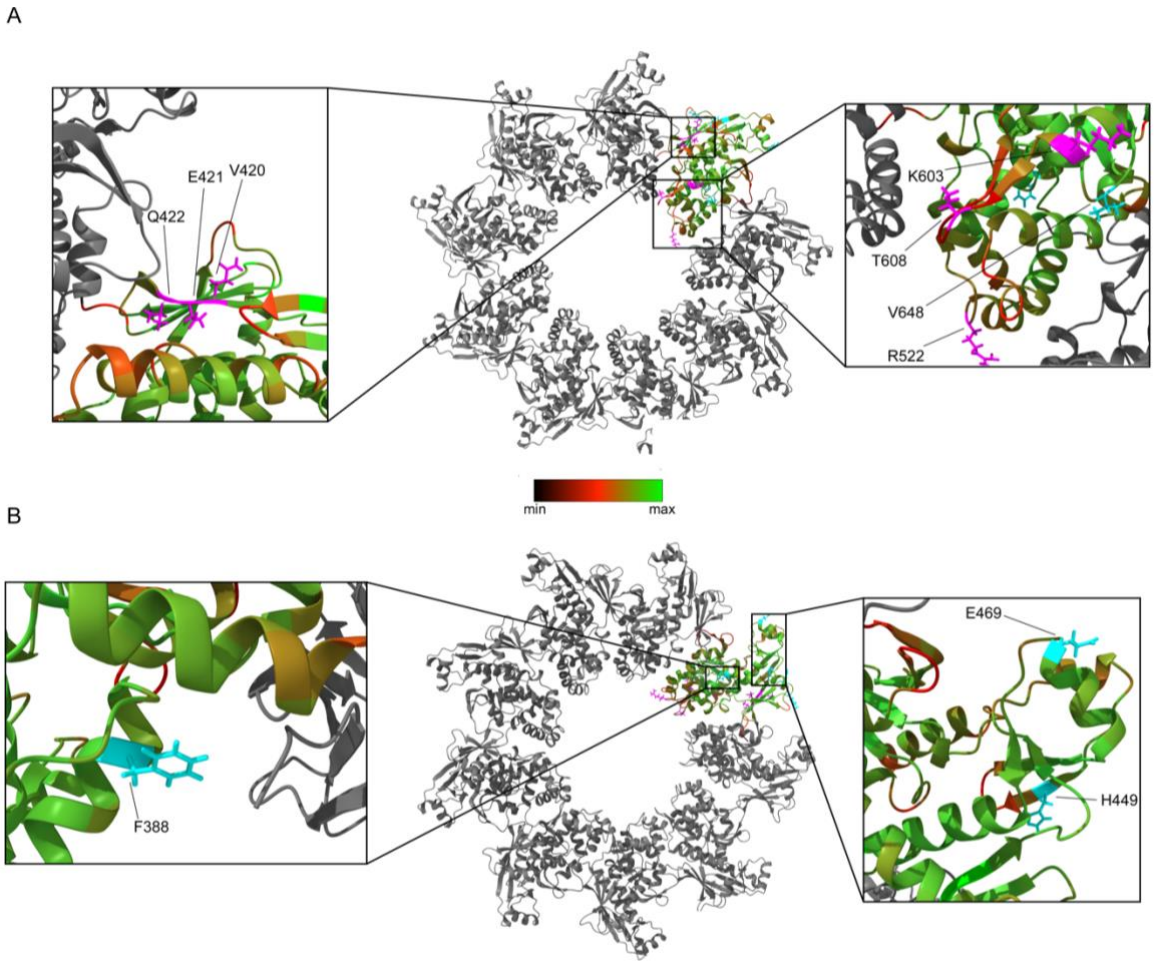

Figure 15 **Crosslinking positions mapped on InvA nonameric structure.** The structure was predicted by AlphaFold for a nonamer of the C-terminal domain (amino acids 357-685) of InvA. One protomer is colored by prediction quality (black: bad quality, red: medium quality, green: high quality). Quantification of the prediction quality for the direct surroundings of the positions can be found in *Table 8*. The atoms of the twelve crosslinking positions are shown as sticks. The positions that abolished secretion and presumably InvA function are depicted in magenta, the functional positions are cyan. **(A)** View from above, looking from the bacterial membrane. On the left are positions V420, E421, and Q422 at the interface between two adjacent protomers. On the right are positions R522, K603, T608, and V648 at the interface between two adjacent protomers. **(B)** View from below, looking from the cytoplasm. On the left is position F388 facing the transmembrane domain (TMD) of a neighboring protomer. On the right are positions H449, and E469 facing the outside of the C-ring.

Analysis of these data provides insights into why several positions might have abolished InvA function: V420, E421, and Q422, which are in close proximity to each other, form a beta sheet according to the AlphaFold prediction. This sheet appears to be part of the interaction site between two adjacent InvA protomers. Mutations at these positions likely disrupt this interaction, leading to an assembly defect visible in the BN data. The other two disruptive mutations, R522 and K603, are located on the opposite side of the protomer, also in the groove between two subunits of the nonamer. The positions T608 and V648, which are in the same area, yielded different outcomes. V648 did not significantly impair InvA function, while T608 results were mixed. Given the prediction quality, particularly for T608, there might be subtle differences in the amino acid locations between the prediction and the actual structure of InvA, causing R522 and K603 to disrupt InvA-InvA interaction, while T608 might only sometimes or partially destabilize the ring, and V648 does not significantly disrupt InvA.

Regarding position F388, the observed crosslinks at approximately 150 kDa and 200 kDa align with the predicted model, where the phenylalanine (F) faces the N-terminal end of an adjacent InvA protomer, near the TMD of the C-ring. This suggests that the 150 kDa crosslink represents an InvA-InvA interaction, corroborated by the size of the crosslink and the high prediction quality for this part of the protein. The 200 kDa crosslink likely indicates an InvA trimer.

The absence of ladders from dimers to nonamers could be attributed to limited efficiency of the photo-crosslinking reaction. Further exploration and optimization of crosslinking conditions, along with complementary techniques, may help to clarify the full interaction landscape between InvA protomers.

Position E469, facing the outside of the protein ring, showed a crosslink at approximately 150 kDa. However, in the predicted nonamer, this position seems too distant to interact with an adjacent protomer. Crosslinking-mass spectrometry analysis could be employed for further characterization of this interaction.

Finally, positions K368 and R370 did not demonstrate functional impairments in InvA and did not exhibit any crosslinks.

For a better overview of the positions tested in this project, refer to Table 8.

Table 8 **Overview of the tested crosslinking positions.** Intermediate (SipD) and late (SipA) secretion is given as mean luminescence in NL assays compared to plasmid-based non-mutated InvA. Italic means statistically insignificantly different to negative control Δ*invA*. Location is based on the AlphaFold prediction of the InvA nonamer. The prediction quality for this structure is the average of the prediction quality scores from AlphaFold for the positions ± 1 amino acid. Values range from 0 (very low quality) to 100 (very high quality).

Position	Paper	SipD secretion [%]	SipA secretion [%]	x-link	Location	Prediction quality
K368	Portaliou	44 ± 31	45 ± 36		Outside of ring	86,2
R370	Portaliou	60 ± 30	49 ± 35		Outside of ring	85,8
F388	Yu	77 ± 35	45 ± 29	X	Next to N-terminus of neighboring protomer	88,4
V420	Portaliou	*1 ± 2*	*1 ±1*		Between protomers	83,8
E421	Portaliou	*2 ± 1*	*2 ± 2*		Between protomers	85,4
Q422	Portaliou	*3 ± 1*	17 ± 6		Between protomers	87,1
H449	Xing	44 ± 13	62 ± 40	X	Outside of ring	84,1
E469	Xing	29 ± 9	62 ± 40		Outside of ring	85
R522	Yu	*2 ± 1*	*2 ± 2*		Between protomers	78,3
K603	Yu	*2 ± 1*	*8 ± 8*		Between protomers	84,8
T608	Yu	10 ± 8	*53 ± 61*		Between protomers	59,3
V648	Yu	30 ± 21	47 ± 41		Between protomers	86,7

6.5 Interaction of InvE and InvA

In this stuy, positions in InvE and InvA were tested based on other studies utilizing peptide arrays, X-ray crystallography, and mutational analysis (Portaliou *et al.*, 2017; Xing *et al.*, 2018; Yu *et al.*, 2018). However, no interaction between InvE and InvA was identified through *in vivo* photocrosslinking. This could be due to either inaccurary of the SctV-SctW hypothesis or limitations of the methods used in his study that would fail to show the interaction. The positions derived from mutational analysis, which exhibited a SctW knockout secretion phenotype in mutated SctV, might represent an indirect method for inferring an interaction between SctV and SctW (Yu *et al.*,

2018). The peptide array approach, offering more direct evidence, showed high signal intensity, increasing confidence in its predictive power (Portaliou *et al.*, 2017).

Notably, interactions between *Shigella's* MxiC and MxiA in a two-hybrid assay (Shen and Blocker, 2016), *Pseudomonas aeruginosa's* PcrQ and PcrD in a coimmunoprecipitation assay (Lee *et al.*, 2014), and SepL and $EscV_C$ in pull-down assays in EPEC (Gaytán et al., 2018) have been observed, supporting the concept of gatekeeper-export apparatus interactions.

Considering these findings, the lack of observed InvE-InvA interactions in this study does not necessarily refute the theory of their interaction. Limitations in the methods used could explain the absence of crosslinks.

For instance, InvE, a cytoplasmic protein thought to bind transiently to the membrane (and specifically to InvA), likely dissociates after the second switch (Kubori and Galán, 2002; Wang *et al.*, 2008; Yu *et al.*, 2018). Capturing this transient interaction at the precise moment during the secretion process presents a biological challenge. The bacteria harvested in the late log phase of this study may not have consistently been in the secretion phase between the first and second switches, where InvA-InvE interaction likely occurs.

The SctV-SctW interaction, if transient, probably has a small contact area. This agrrees with the observation that more conserved interaction sites typically involve fewer surface residues, which need to be maintained during evolution (Nooren and Thornton, 2003). A smaller surface area is also more energetically favorable (Chen, Sawyer and Regan, 2013). On the flipside, this would mean that the establishment of such an interaction might take less time. Capturing such a brief moment of interaction might be challenging.

Additionally, the investigated residue must be very close to its binding partner, within 6 Å of the position of the aryl ring of the *p*Bpa (Chin *et al.*, 2002). It might be that SctV and SctW interact, but that the tested positions are simply too far away from its binding partner, posing a molecular limitation of the photocrosslinking method.

Another technical limiting factor is the detection of crosslinks by immunoblotting, because of limited transfer efficiency and sensitivity of detection (Stott, 1989). It might be that SctV-SctW interactions do take place in the tested samples, but this experiment's means of detection are simply not sensitive enough.

Taken together, no interaction between InvE and InvA was identified, which may be attributed to biological, molecular, or technical limitations.

To enhance the experimental setup, testing switching mutants like Δ*sctP* or $SctU_{N258A}$ could be beneficial as they stabilize the T3SS in specific states, reducing uncertainty about the bacteria's state during secretion. This approach could provide a more detailed understanding of the timing of InvE-InvA interactions and the precise conditions necessary for InvE binding and release.

Additional positions identified in the literature could be examined using *in vivo* photocrosslinking and mass spectrometry to further probe these interactions. Alternatively, techniques such as co-immunoprecipitation or surface plasmon resonance (SPR) studies could offer additional insights into the nature of these protein-protein interactions (Berggård, Linse and James, 2007).

6.6 Concluding remarks

In total, although some interactions of InvA with InvA and some unidentified protein could be established, this study could not substantiate a potential interaction between InvA and InvE. This study has confirmed and quantified the Δ*invE* secretion phenotype and hinted at the importance of the N-terminal secretion signal of InvE. The gatekeeper undoubtedly plays an integral part in establishing the secretion hierarchy and in substrate specificity switching between intermediate and late secretion. Additionally, data from this study identified regions in InvA that are important for overall function of the T3SS. However, the findings are not yet conclusive regarding a gatekeeper mechanism. The study proposes enhancements for future experimental approaches and outlines potential avenues for continued scientific inquiry.

7 Summary

Type III Secretion Systems (T3SS) are a key factor to the virulence of *Salmonella* Typhimurium. They are membrane-spanning syringe-like molecular machines that inject effector proteins through a hollow needle-like filament directly into the target cells. One prominent hallmark of T3SS is the secretion hierarchy, with distinct stages of assembly and secretion that follow a strict sequential and temporal order. InvE, the Salmonella pathogenicity island-1 (SPI-1) homolog of SctW, is thought to be a vital regulator for the switch between intermediate and late substrates. The so-called gatekeeper is thought to block substrate specificity switching until host cell contact is established. It is suggested that interaction of SctW with the major export apparatus protein InvA, the SPI-1 homolog of SctV, is vital for the regulation of secretion, and several positions in SctW and SctV have been proposed as part of the interaction interface. The aim of this study was to investigate this interaction and the role of InvE as a gatekeeper. The secretion phenotype of Δ*invE* was assessed with a NanoLuc (NL) luciferase-based T3SS secretion assay. The findings in this study agree with previous data and additionally, newly quantify the abolishment of translocators and oversecretion of effectors in a variety of contexts. Additionally, it was found that tagging of the N-terminus interfered with InvE function, whereas C-terminal tagging can be used for further studies. The results hint at the importance of the N-terminal secretion signal of InvE. Several mutants of specific amino acid residues in InvA have been assessed for their secretion phenotype by NL and TCA-based secretion assays, for protein expression by SDS-PAGE, and for assembly by BN PAGE. The positions were mapped on a predicted nonameric ring structure of InvA and identify regions that are essential for overall function of the T3SS. Interaction between InvA and InvE was investigated by *in vivo* photocrosslinking. Although some interactions of InvA with other proteins could be identified, no interaction between these two proteins could be identified. The study confirms that the gatekeeper undoubtedly plays an integral part in establishing the secretion hierarchy and in substrate specificity switching between intermediate and late secretion. Nevertheless, the data is incomplete and cannot confirm a possible gatekeeper

mechanism, but rather suggests possible improvements for further experiments and options for further scientific exploration.

8 Deutsche Zusammenfassung

Typ-III-Sekretionssysteme (T3SS) sind ein wesentlicher Faktor für die Virulenz von *Salmonella* Typhimurium. Diese molekularen Maschinen können Effektorproteine mittels einer Nadelstrukur über Membranen hinweg direkt in Zielzellen injizieren. Ein besonderes Merkmal der T3SS ist die Sekretionshierarchie, durch die verschiedene Phasen des T3SS-Aufbaus und der Sekretion in einer strikten zeitlichen Abfolge verlaufen. InvE, das Homolog von SctW in der *Salmonella*-Pathogenitätsinsel-1 (SPI-1), ist ein wichtiger Regulator für den Wechsel zwischen den intermediären und späten Substraten. Es wird angenommen, dass das sogennante gatekeeper-Protein (engl. Pförtner, Türsteher) InvE den Wechsel zwischen den Substraten blockiert, bis ein Kontakt mit der Wirtszelle hergestellt ist. Vermutlich ist die Interaktion von InvE mit dem Hauptprotein des Exportapparats InvA, dem SPI-1-Homologen von SctV, für die Regulierung der Sekretion von entscheidender Bedeutung. In dieser Studie sollten diese Interaktion und die Rolle von InvE als gatekeeper-Protein untersucht werden. Der Sekretionsphänotyp von Δ*invE* wurde mit einem NanoLuc (NL) Luciferase-basierten T3SS-Sekretionstest untersucht. Die Ergebnisse dieser Studie stimmen mit früheren Daten überein und quantifizieren zusätzlich die Unterdrückung der Sekretion von intermediären Substraten und die Übersekretion von Effektoren in neuen Kontexten. Die Markierung des C-Terminus von InvE kann für weitere Studien genutzt werden, wohingegen die Markierung des N-Terminus die InvE-Funktion einschränkt und so auf dessen Bedeutung hinweist. Mehrere Mutanten verschiedener Aminosäurereste in InvA wurden auf ihren Sekretionsphänotyp, auf ihre Proteinexpression und auf den T3SS-Aufbau hin untersucht. In Zusammenschau mit einer vorhergesagten nonameren Ringstruktur von InvA wurden Regionen in InvA identifiziert, die für die Gesamtfunktion des T3SS wesentlich sind. Die Interaktion zwischen InvA und InvE wurde durch *in vivo* Photocrosslinking untersucht. Obwohl zwei Interaktionen von InvA mit anderen

Proteinen detektiert werden konnten, wurde keine Interaktion zwischen InvA und InvE festgestellt. Die Studie bestätigt die wesentliche Rolle von InvE in der Sekretionshierarchie und bei dem Wechsel zwischen intermediärer und später Sekretion. Dennoch sind die Daten unvollständig und können einen möglichen gatekeeper-Mechanismus nicht herleiten. Vielmehr werden Verbesserungsmöglichkeiten für weitere Experimente und Optionen für die weitere Forschung aufgezeigt.

Literature

Abrusci, P. *et al.* (2013) 'Architecture of the major component of the type III secretion system export apparatus', *Nature Structural & Molecular Biology*, 20(1), pp. 99–104. doi: 10.1038/nsmb.2452.

Agilent Technologies (no date) 'QuikChange II Site-Directed Mutagenesis Kit - Instruction Manual', *Revision E.0*.

Akeda, Y. and Galán, J. E. (2005) 'Chaperone release and unfolding of substrates in type III secretion', *Nature*, 437(7060), pp. 911–915. doi: 10.1038/nature03992.

Archuleta, T. L. *et al.* (2011) 'The Chlamydia Effector Chlamydial Outer Protein N (CopN) Sequesters Tubulin and Prevents Microtubule Assembly', *Journal of Biological Chemistry*, 286(39), pp. 33992–33998. doi: 10.1074/jbc.M111.258426.

Berggård, T., Linse, S. and James, P. (2007) 'Methods for the detection and analysis of protein–protein interactions', *PROTEOMICS*, 7(16), pp. 2833–2842. doi: 10.1002/pmic.200700131.

Boland A, S. M. I. M. K. C. W. P. C. GR. (1996) 'Status of YopM and YopN in the Yersinia Yop virulon: YopM of Y.enterocolitica is internalized inside the cytosol of PU5-1.8 macrophages by the YopB, D, N delivery apparatus', *EMBO J.*, 15(19), pp. 5191–5201.

Botteaux, A. *et al.* (2009) 'MxiC is secreted by and controls the substrate specificity of the *Shigella flexneri* type III secretion apparatus', *Molecular Microbiology*, 71(2), pp. 449–460. doi: 10.1111/j.1365-2958.2008.06537.x.

Broz, P. *et al.* (2007) 'Function and molecular architecture of the Yersinia injectisome tip complex', *Molecular Microbiology*, 65(5), pp. 1311–1320. doi: 10.1111/j.1365-2958.2007.05871.x.

Burkinshaw, B. J., Souza, S. A. and Strynadka, N. C. J. (2015) 'Structural analysis of SepL, an enteropathogenic *Escherichia coli* type III secretion-system

gatekeeper protein', *Acta Crystallographica Section F Structural Biology Communications*, 71(10), pp. 1300–1308. doi: 10.1107/S2053230X15016064.

Büttner, D. (2012) 'Protein Export According to Schedule: Architecture, Assembly, and Regulation of Type III Secretion Systems from Plant- and Animal-Pathogenic Bacteria', *Microbiology and Molecular Biology Reviews*, 76(2), pp. 262–310. doi: 10.1128/MMBR.05017-11.

Chen, J., Sawyer, N. and Regan, L. (2013) 'Protein-protein interactions: General trends in the relationship between binding affinity and interfacial buried surface area', *Protein Science*, 22(4), pp. 510–515. doi: 10.1002/pro.2230.

Cherradi, Y. *et al.* (2013) 'Interplay between predicted inner-rod and gatekeeper in controlling substrate specificity of the type III secretion system', *Molecular Microbiology*, 87(6), pp. 1183–1199. doi: 10.1111/mmi.12158.

Chevance, F. F. v. and Hughes, K. T. (2008) 'Coordinating assembly of a bacterial macromolecular machine', *Nature Reviews Microbiology*, 6(6), pp. 455–465. doi: 10.1038/nrmicro1887.

Chin, J. W. *et al.* (2002) 'Addition of a photocrosslinking amino acid to the genetic code of *Escherichia coli*', *Proceedings of the National Academy of Sciences*, 99(17), pp. 11020–11024. doi: 10.1073/pnas.172226299.

Costa, T. R. D. *et al.* (2015a) 'Secretion systems in Gram-negative bacteria: structural and mechanistic insights', *Nature Reviews Microbiology*, 13(6), pp. 343–359. doi: 10.1038/nrmicro3456.

Costa, T. R. D. *et al.* (2015b) 'Secretion systems in Gram-negative bacteria: structural and mechanistic insights', *Nature Reviews Microbiology*, 13(6), pp. 343–359. doi: 10.1038/nrmicro3456.

Cui, S. *et al.* (2008) 'Ciprofloxacin-Resistant *Salmonella enterica* Serotype Typhimurium, China', *Emerging Infectious Diseases*, 14(3), pp. 493–495. doi: 10.3201/eid1403.070857.

Deane, J. E. *et al.* (2008a) 'Structures of the Shigella flexneri Type 3 Secretion System Protein MxiC Reveal Conformational Variability Amongst Homologues',

Journal of Molecular Biology, 377(4), pp. 985–992. doi: 10.1016/j.jmb.2008.01.072.

Deane, J. E. *et al.* (2008b) 'Structures of the Shigella flexneri Type 3 Secretion System Protein MxiC Reveal Conformational Variability Amongst Homologues', *Journal of Molecular Biology*, 377(4), pp. 985–992. doi: 10.1016/j.jmb.2008.01.072.

Deane, J. E. *et al.* (2010) 'Timing is everything: the regulation of type III secretion', *Cellular and Molecular Life Sciences*, 67(7), pp. 1065–1075. doi: 10.1007/s00018-009-0230-0.

Deng, W. *et al.* (2004) 'Dissecting virulence: Systematic and functional analyses of a pathogenicity island', *Proceedings of the National Academy of Sciences*, 101(10), pp. 3597–3602. doi: 10.1073/pnas.0400326101.

Deng, W. *et al.* (2005a) 'Regulation of Type III Secretion Hierarchy of Translocators and Effectors in Attaching and Effacing Bacterial Pathogens', *Infection and Immunity*, 73(4), pp. 2135–2146. doi: 10.1128/IAI.73.4.2135-2146.2005.

Deng, W. *et al.* (2005b) 'Regulation of Type III Secretion Hierarchy of Translocators and Effectors in Attaching and Effacing Bacterial Pathogens', *Infection and Immunity*, 73(4), pp. 2135–2146. doi: 10.1128/IAI.73.4.2135-2146.2005.

Deng, W. *et al.* (2017) 'Assembly, structure, function and regulation of type III secretion systems', *Nature Reviews Microbiology*, 15(6), pp. 323–337. doi: 10.1038/nrmicro.2017.20.

Diepold, A. and Wagner, S. (2014) 'Assembly of the bacterial type III secretion machinery', *FEMS Microbiology Reviews*, 38(4), pp. 802–822. doi: 10.1111/1574-6976.12061.

Dietsche, T. *et al.* (2016) 'Structural and Functional Characterization of the Bacterial Type III Secretion Export Apparatus', *PLOS Pathogens*, 12(12), p. e1006071. doi: 10.1371/journal.ppat.1006071.

Dower, W. J., Miller, J. F. and Ragsdale, C. W. (1988) ‘High efficiency transformation of E.coli by high voltage electroporation’, *Nucleic Acids Research*, 16(13), pp. 6127–6145. doi: 10.1093/nar/16.13.6127.

Ehuwa, O., Jaiswal, A. K. and Jaiswal, S. (2021) ‘Salmonella, Food Safety and Food Handling Practices’, *Foods*, 10(5), p. 907. doi: 10.3390/foods10050907.

Ellermeier, C. D., Ellermeier, J. R. and Slauch, J. M. (2005) ‘HilD, HilC and RtsA constitute a feed forward loop that controls expression of the SPI1 type three secretion system regulator hilA in Salmonella enterica serovar Typhimurium’, *Molecular Microbiology*, 57(3), pp. 691–705. doi: 10.1111/j.1365-2958.2005.04737.x.

Fatica, M. K. and Schneider, K. R. (2011) ‘Salmonella and produce: Survival in the plant environment and implications in food safety’, *Virulence*, 2(6), pp. 573–579. doi: 10.4161/viru.2.6.17880.

Ferracci, F. *et al.* (2005) ‘Selection and characterization of Yersinia pestis YopN mutants that constitutively block Yop secretion’, *Molecular Microbiology*, 57(4), pp. 970–987. doi: 10.1111/j.1365-2958.2005.04738.x.

Forsberg, Å. *et al.* (1991) ‘The surface-located YopN protein is involved in calcium signal transduction in *Yersinia pseudotuberculosis*’, *Molecular Microbiology*, 5(4), pp. 977–986. doi: 10.1111/j.1365-2958.1991.tb00773.x.

Galán, J. E. *et al.* (2014) ‘Bacterial Type III Secretion Systems: Specialized Nanomachines for Protein Delivery into Target Cells’, *Annual Review of Microbiology*, 68(1), pp. 415–438. doi: 10.1146/annurev-micro-092412-155725.

Galán, J. E. and Waksman, G. (2018) ‘Protein-Injection Machines in Bacteria’, *Cell*. Cell Press, pp. 1306–1318. doi: 10.1016/j.cell.2018.01.034.

Gal-Mor, O. and Finlay, B. B. (2006) ‘Pathogenicity islands: a molecular toolbox for bacterial virulence’, *Cellular Microbiology*, 8(11), pp. 1707–1719. doi: 10.1111/j.1462-5822.2006.00794.x.

Gaytán, M. O. *et al.* (2018) 'Novel insights into the mechanism of SepL-mediated control of effector secretion in enteropathogenic *Escherichia coli*', *MicrobiologyOpen*, 7(3), p. e00571. doi: 10.1002/mbo3.571.

Gibson, D. G. *et al.* (2009) 'Enzymatic assembly of DNA molecules up to several hundred kilobases', *Nature Methods*, 6(5), pp. 343–345. doi: 10.1038/nmeth.1318.

Ginocchio, C., Pace, J. and Galán, J. E. (1992) 'Identification and molecular characterization of a Salmonella typhimurium gene involved in triggering the internalization of salmonellae into cultured epithelial cells.', *Proceedings of the National Academy of Sciences*, 89(13), pp. 5976–5980. doi: 10.1073/pnas.89.13.5976.

Groisman, E. A. and Ochman, H. (1996) 'Pathogenicity Islands: Bacterial Evolution in Quantum Leaps', *Cell*, 87(5), pp. 791–794. doi: 10.1016/S0092-8674(00)81985-6.

Grossman, A. S. *et al.* (2021) 'A Widespread Bacterial Secretion System with Diverse Substrates', *mBio*, 12(4). doi: 10.1128/mBio.01956-21.

Håkansson S, S. K. P. C. G. E. R. R. H. F. W.-W. H. (1996) 'The YopB protein of Yersinia pseudotuberculosis is essential for the translocation of Yop effector proteins across the target cell plasma membrane and displays a contact-dependent membrane disrupting activity.', *EMBO J.*, 15(21), pp. 5812–5823.

HEINITZ, M. L. *et al.* (2000) 'Incidence of Salmonella in Fish and Seafood†', *Journal of Food Protection*, 63(5), pp. 579–592. doi: 10.4315/0362-028X-63.5.579.

Hueck, C. J. (1998) 'Type III Protein Secretion Systems in Bacterial Pathogens of Animals and Plants', *Microbiology and Molecular Biology Reviews*, 62(2), pp. 379–433. doi: 10.1128/MMBR.62.2.379-433.1998.

Iriarte, M. *et al.* (1998) 'TyeA, a protein involved in control of Yop release and in translocation of Yersinia Yop effectors', *The EMBO Journal*, 17(7), pp. 1907–1918. doi: 10.1093/emboj/17.7.1907.

Journet, L. *et al.* (2003) ‘The Needle Length of Bacterial Injectisomes Is Determined by a Molecular Ruler’, *Science*, 302(5651), pp. 1757–1760. doi: 10.1126/science.1091422.

Jumper, J. *et al.* (2021) ‘Highly accurate protein structure prediction with AlphaFold’, *Nature*, 596(7873), pp. 583–589. doi: 10.1038/s41586-021-03819-2.

Kaniga, K., Bossio, J. C. and Galán, J. E. (1994) ‘The Salmonella typhimurium invasion genes invF and invG encode homologues of the AraC and PulD family of proteins’, *Molecular Microbiology*, 13(4), pp. 555–568. doi: 10.1111/j.1365-2958.1994.tb00450.x.

Kim, J. S. *et al.* (2013) ‘Molecular characterization of the InvE regulator in the secretion of type III secretion translocases in Salmonella enterica serovar Typhimurium’, *Microbiology*, 159(Pt_3), pp. 446–461. doi: 10.1099/mic.0.061689-0.

Kimbrough, T. G. and Miller, S. I. (2000) ‘Contribution of *Salmonella typhimurium* type III secretion components to needle complex formation’, *Proceedings of the National Academy of Sciences*, 97(20), pp. 11008–11013. doi: 10.1073/pnas.200209497.

Kresse, A. U. *et al.* (2000) ‘Characterization of SepL of Enterohemorrhagic *Escherichia coli*’, *Journal of Bacteriology*, 182(22), pp. 6490–6498. doi: 10.1128/JB.182.22.6490-6498.2000.

Kubori, T. *et al.* (1998) ‘Supramolecular Structure of the *Salmonella typhimurium* Type III Protein Secretion System’, *Science*, 280(5363), pp. 602–605. doi: 10.1126/science.280.5363.602.

Kubori, T. *et al.* (2000) ‘Molecular characterization and assembly of the needle complex of the *Salmonella typhimurium* type III protein secretion system’, *Proceedings of the National Academy of Sciences*, 97(18), pp. 10225–10230. doi: 10.1073/pnas.170128997.

Kubori, T. and Galán, J. E. (2002) ‘*Salmonella* Type III Secretion-Associated Protein InvE Controls Translocation of Effector Proteins into Host Cells’, *Journal*

of Bacteriology, 184(17), pp. 4699–4708. doi: 10.1128/JB.184.17.4699-4708.2002.

Kuhlen, L. *et al.* (2018) 'Structure of the core of the type III secretion system export apparatus', *Nature Structural & Molecular Biology*, 25(7), pp. 583–590. doi: 10.1038/s41594-018-0086-9.

Kvitko, B. H. *et al.* (2012) 'A simple method for construction of pir + Enterobacterial hosts for maintenance of R6K replicon plasmids', *BMC Research Notes*, 5(1), p. 157. doi: 10.1186/1756-0500-5-157.

Lara-Tejero, M. *et al.* (2011) 'A Sorting Platform Determines the Order of Protein Secretion in Bacterial Type III Systems', *Science*, 331(6021), pp. 1188–1191. doi: 10.1126/science.1201476.

Lee, P.-C. *et al.* (2014) 'Control of type III secretion activity and substrate specificity by the cytoplasmic regulator PcrG', *Proceedings of the National Academy of Sciences*, 111(19). doi: 10.1073/pnas.1402658111.

Liu, W. *et al.* (2007) 'Structural Basis for the Recognition ofpara-Benzoyl-L-phenylalanine by Evolved Aminoacyl-tRNA Synthetases', *Angewandte Chemie International Edition*, 46(32), pp. 6073–6075. doi: 10.1002/anie.200701990.

Loquet, A. *et al.* (2012) 'Atomic model of the type III secretion system needle', *Nature*, 486(7402), pp. 276–279. doi: 10.1038/nature11079.

Majewski, D. D. *et al.* (2020) 'Cryo-EM analysis of the SctV cytosolic domain from the enteropathogenic E. coli T3SS injectisome', *Journal of Structural Biology*, 212(3), p. 107660. doi: 10.1016/j.jsb.2020.107660.

Majowicz, S. E. *et al.* (2010) 'The Global Burden of Nontyphoidal *Salmonella* Gastroenteritis', *Clinical Infectious Diseases*, 50(6), pp. 882–889. doi: 10.1086/650733.

Marlovits, T. C. *et al.* (2006) 'Assembly of the inner rod determines needle length in the type III secretion injectisome', *Nature*, 441(7093), pp. 637–640. doi: 10.1038/nature04822.

Martinez-Argudo, I. and Blocker, A. J. (2010) ‘The Shigella T3SS needle transmits a signal for MxiC release, which controls secretion of effectors’, *Molecular Microbiology*, 78(6), pp. 1365–1378. doi: 10.1111/j.1365-2958.2010.07413.x.

McShan, A. C. and de Guzman, R. N. (2015) ‘The Bacterial Type III Secretion System as a Target for Developing New Antibiotics’, *Chemical Biology & Drug Design*, 85(1), pp. 30–42. doi: 10.1111/cbdd.12422.

MEYER, C. *et al.* (2010) ‘Salmonella in Raw Meat and By-Products from Pork and Beef’, *Journal of Food Protection*, 73(10), pp. 1780–1784. doi: 10.4315/0362-028X-73.10.1780.

Monjarás Feria, J. V. *et al.* (2015) ‘Role of Autocleavage in the Function of a Type III Secretion Specificity Switch Protein in Salmonella enterica Serovar Typhimurium’, *mBio*, 6(5). doi: 10.1128/mBio.01459-15.

Mota, L. J., Sorg, I. and Cornelis, G. R. (2005) ‘Type III secretion: The bacteria-eukaryotic cell express’, *FEMS Microbiology Letters*, 252(1), pp. 1–10. doi: 10.1016/j.femsle.2005.08.036.

Nawrotek, A. *et al.* (2014) ‘Biochemical and Structural Insights into Microtubule Perturbation by CopN from Chlamydia pneumoniae’, *Journal of Biological Chemistry*, 289(36), pp. 25199–25210. doi: 10.1074/jbc.M114.568436.

Nooren, I. M. A. and Thornton, J. M. (2003) ‘Structural Characterisation and Functional Significance of Transient Protein–Protein Interactions’, *Journal of Molecular Biology*, 325(5), pp. 991–1018. doi: 10.1016/S0022-2836(02)01281-0.

Ochman, H., Lawrence, J. G. and Groisman, E. A. (2000) ‘Lateral gene transfer and the nature of bacterial innovation’, *Nature*, 405(6784), pp. 299–304. doi: 10.1038/35012500.

O’Connell, C. B. *et al.* (2004) ‘SepL, a protein required for enteropathogenic Escherichia coli type III translocation, interacts with secretion component SepD’,

Molecular Microbiology, 52(6), pp. 1613–1625. doi: 10.1111/j.1365-2958.2004.04101.x.

Pallen, M. J., Beatson, S. A. and Bailey, C. M. (2005) 'Bioinformatics, genomics and evolution of non-flagellar type-III secretion systems: a Darwinian perpective', *FEMS Microbiology Reviews*, 29(2), pp. 201–229. doi: 10.1016/j.femsre.2005.01.001.

Patra, S. D. *et al.* (2021) 'Prevalence and multidrug resistance in Salmonella enterica Typhimurium: an overview in South East Asia', *World Journal of Microbiology and Biotechnology*, 37(11), p. 185. doi: 10.1007/s11274-021-03146-8.

Portaliou, A. G. *et al.* (2016) 'Type III Secretion: Building and Operating a Remarkable Nanomachine', *Trends in Biochemical Sciences*, 41(2), pp. 175–189. doi: 10.1016/j.tibs.2015.09.005.

Portaliou, A. G. *et al.* (2017) 'Hierarchical protein targeting and secretion is controlled by an affinity switch in the type <scp>III</scp> secretion system of enteropathogenic *Escherichia coli*', *The EMBO Journal*, 36(23), pp. 3517–3531. doi: 10.15252/embj.201797515.

Roehrich, A. D. *et al.* (2017) 'Steps for Shigella Gatekeeper Protein MxiC Function in Hierarchical Type III Secretion Regulation', *Journal of Biological Chemistry*, 292(5), pp. 1705–1723. doi: 10.1074/jbc.M116.746826.

Ryu, Y. and Schultz, P. G. (2006) 'Efficient incorporation of unnatural amino acids into proteins in Escherichia coli', *Nature Methods*, 3(4), pp. 263–265. doi: 10.1038/nmeth864.

Samudrala, R., Heffron, F. and McDermott, J. E. (2009) 'Accurate Prediction of Secreted Substrates and Identification of a Conserved Putative Secretion Signal for Type III Secretion Systems', *PLoS Pathogens*, 5(4), p. e1000375. doi: 10.1371/journal.ppat.1000375.

dos Santos, A. M. P., Ferrari, R. G. and Conte-Junior, C. A. (2020) ‘Type three secretion system in Salmonella Typhimurium: the key to infection’, *Genes & Genomics*, 42(5), pp. 495–506. doi: 10.1007/s13258-020-00918-8.

Schubot, F. D. *et al.* (2005) ‘Three-dimensional Structure of a Macromolecular Assembly that Regulates Type III Secretion in Yersinia pestis’, *Journal of Molecular Biology*, 346(4), pp. 1147–1161. doi: 10.1016/j.jmb.2004.12.036.

Schubot, F. D. *et al.* (2009) ‘Crystal structure of the protease-resistant core domain of Yersinia pestis virulence factor YopR’, *Protein Science*, 14(6), pp. 1679–1683. doi: 10.1110/ps.051446405.

Shaulov, L. *et al.* (2017) ‘The Ruler Protein EscP of the Enteropathogenic *Escherichia coli* Type III Secretion System Is Involved in Calcium Sensing and Secretion Hierarchy Regulation by Interacting with the Gatekeeper Protein SepL’, *mBio*, 8(1). doi: 10.1128/mBio.01733-16.

Shen, D.-K. and Blocker, A. J. (2016) ‘MxiA, MxiC and IpaD Regulate Substrate Selection and Secretion Mode in the T3SS of Shigella flexneri’, *PLOS ONE*, 11(5), p. e0155141. doi: 10.1371/journal.pone.0155141.

Silva-Herzog, E. *et al.* (2011) ‘Scc1 (CP0432) and Scc4 (CP0033) Function as a Type III Secretion Chaperone for CopN of Chlamydia pneumoniae’, *Journal of Bacteriology*, 193(14), pp. 3490–3496. doi: 10.1128/JB.00203-11.

Singh, N. and Wagner, S. (2019) ‘Investigating the assembly of the bacterial type III secretion system injectisome by in vivo photocrosslinking’, *International Journal of Medical Microbiology*, 309(6), p. 151331. doi: 10.1016/j.ijmm.2019.151331.

Stott, D. I. (1989) ‘Immunoblotting and dot blotting’, *Journal of Immunological Methods*, 119(2), pp. 153–187. doi: 10.1016/0022-1759(89)90394-3.

Sukhan, A. *et al.* (2001a) ‘Genetic Analysis of Assembly of the *Salmonella enterica* Serovar Typhimurium Type III Secretion-Associated Needle Complex’, *Journal of Bacteriology*, 183(4), pp. 1159–1167. doi: 10.1128/JB.183.4.1159-1167.2001.

Sukhan, A. *et al.* (2001b) ‘Genetic Analysis of Assembly of the *Salmonella enterica* Serovar Typhimurium Type III Secretion-Associated Needle Complex’, *Journal of Bacteriology*, 183(4), pp. 1159–1167. doi: 10.1128/JB.183.4.1159-1167.2001.

Sundberg, L. and Forsberg, A. (2003) ‘TyeA of Yersinia pseudotuberculosis is involved in regulation of Yop expression and is required for polarized translocation of Yop effectors’, *Cellular Microbiology*, 5(3), pp. 187–202. doi: 10.1046/j.1462-5822.2003.00267.x.

Teitzel, G. (2013) ‘Taking the first steps towards infection’, *Trends in Microbiology*, 21(8), p. 359. doi: 10.1016/j.tim.2013.06.007.

Tosi, T. *et al.* (2013) ‘Structural basis of eukaryotic cell targeting by type III secretion system (T3SS) effectors’, *Research in Microbiology*, 164(6), pp. 605–619. doi: 10.1016/j.resmic.2013.03.019.

Varadi, M. *et al.* (2022) ‘AlphaFold Protein Structure Database: massively expanding the structural coverage of protein-sequence space with high-accuracy models’, *Nucleic Acids Research*, 50(D1), pp. D439–D444. doi: 10.1093/nar/gkab1061.

Wagner, S. *et al.* (2010) ‘Organization and coordinated assembly of the type III secretion export apparatus’, *Proceedings of the National Academy of Sciences*, 107(41), pp. 17745–17750. doi: 10.1073/pnas.1008053107.

Wagner, S. *et al.* (2018) ‘Bacterial type III secretion systems: a complex device for the delivery of bacterial effector proteins into eukaryotic host cells’, *FEMS Microbiology Letters*, 365(19). doi: 10.1093/femsle/fny201.

Wagner, S. and Diepold, A. (2020) ‘A Unified Nomenclature for Injectisome-Type Type III Secretion Systems’, in, pp. 1–10. doi: 10.1007/82_2020_210.

Wang, D. *et al.* (2008) ‘Hierarchal type III secretion of translocators and effectors from *Escherichia coli* O157:H7 requires the carboxy terminus of SepL that binds to Tir’, *Molecular Microbiology*, 69(6), pp. 1499–1512. doi: 10.1111/j.1365-2958.2008.06377.x.

Westerhausen, S. *et al.* (2020) ‘A NanoLuc luciferase-based assay enabling the real-time analysis of protein secretion and injection by bacterial type III secretion systems’, *Molecular Microbiology*, 113(6), pp. 1240–1254. doi: 10.1111/mmi.14490.

WHO (2015) *WHO estimates of the global burden of foodborne diseases: foodborne disease burden epidemiology reference group 2007-2015*.

WHO (2018) *WHO Fact sheet ‘Salmonella (non-typhoidal)’ [https://www.who.int/news-room/fact-sheets/detail/salmonella-(non-typhoidal)]*.

Wilharm, G. *et al.* (2004) ‘*Yersinia enterocolitica* Type III Secretion Depends on the Proton Motive Force but Not on the Flagellar Motor Components MotA and MotB’, *Infection and Immunity*, 72(7), pp. 4004–4009. doi: 10.1128/IAI.72.7.4004-4009.2004.

Worrall, L. J., Vuckovic, M. and Strynadka, N. C. J. (2010) ‘Crystal structure of the C-terminal domain of the *Salmonella* type III secretion system export apparatus protein InvA’, *Protein Science*, 19(5), pp. 1091–1096. doi: 10.1002/pro.382.

Xing, Q. *et al.* (2018) ‘Structures of chaperone-substrate complexes docked onto the export gate in a type III secretion system’, *Nature Communications*, 9(1), p. 1773. doi: 10.1038/s41467-018-04137-4.

Younis, R. *et al.* (2010) ‘SepL Resembles an Aberrant Effector in Binding to a Class 1 Type III Secretion Chaperone and Carrying an N-Terminal Secretion Signal’, *Journal of Bacteriology*, 192(22), pp. 6093–6098. doi: 10.1128/JB.00760-10.

Yu, X. J. *et al.* (2018) ‘Ssav interacts with SsaL to control the translocon-to-effector switch in the salmonella SPI-2 type three secretion system’, *mBio*, 9(5). doi: 10.1128/mBio.01149-18.

Yu, X.-J. *et al.* (2010) ‘pH Sensing by Intracellular *Salmonella* Induces Effector Translocation’, *Science*, 328(5981), pp. 1040–1043. doi: 10.1126/science.1189000.

Yu, X.-J., Liu, M. and Holden, D. W. (2004) ‘SsaM and SpiC interact and regulate secretion of Salmonella Pathogenicity Island 2 type III secretion system effectors and translocators’, *Molecular Microbiology*, 54(3), pp. 604–619. doi: 10.1111/j.1365-2958.2004.04297.x.

Zilkenat, S. *et al.* (2016) ‘Determination of the Stoichiometry of the Complete Bacterial Type III Secretion Needle Complex Using a Combined Quantitative Proteomic Approach’, *Molecular & Cellular Proteomics*, 15(5), pp. 1598–1609. doi: 10.1074/mcp.M115.056598.

9 Erklärung zum Eigenanteil

Die Arbeit wurde im Interfakultären Institut für Mikrobiologie und Infektionsmedizin unter Betreuung von Prof. Samuel Wagner und Mentorat von Dr. Iwan Grin durchgeführt. Die Konzeption der Studie erfolgte in Zusammenarbeit mit Samuel Wagner, Professor für Infektionsbiologie. Sämtliche Versuche wurden nach Einarbeitung durch Labormitglieder Andrea Eipper, Dr. Iwan Grin, Dr. Nidhi Singh und Dr. Sibel Westerhausen von mir eigenständig durchgeführt. Die statistische Auswertung erfolgte nach Beratung von Dr. Ulrich Schoppmeier eigenständig durch mich. Sämtliche Grafiken wurden, sofern nicht anders vermerkt, eigenständig erstellt. Ich versichere, das Manuskript selbständig verfasst zu haben und keine weiteren als die von mir angegebenen Quellen verwendet zu haben. Die aus fremden Quellen direkt oder indirekt übernommenen Gedanken sind ausnahmslos als solche kenntlich gemacht. Anmerkungen zum Manuskript erfolgten durch Dr. Iwan Grin und Prof. Samuel Wagner.

Clara Schönwald

Tübingen, den 21.12.2023

10 Danksagung

Zuletzt möchte ich allen danken, die zum Gelingen dieser Dissertation beigetragen haben.

Mein besonderer Dank gilt Samuel. Du warst der Doktorvater, den ich mir gewünscht habe, und trotz deines vollen Terminkalenders hast du dir für mich und meine Fragen immer Zeit genommen. Außerdem hast du eine wirklich fantastische Arbeitsgruppe aufgebaut.

Ein großer Dank geht auch an Iwan. Du hast die Rolle als Betreuer perfekt ausgefüllt, auch wenn du diese Rolle auf dem Papier gar nicht hattest. Auf dich konnte ich immer zählen, ob zum PCR-Trouble-Shooting, für aufbauende Worte oder konstruktive Anmerkungen.

Außerdem einen großen Dank an die gesamte Arbeitsgruppe Wagner. Das Jahr, das ich im Labor verbracht habe ist mir in bester Erinnerung geblieben. Die Arbeitsatmosphäre ist für mich immer noch der Goldstandard für jede weitere Beschäftigung. Danke an Andrea, die mir im Labor immer weiterhelfen konnte. Du bist eine große Bereicherung für das ganze Team und hältst so viele Fäden zusammen. Danke an Sibel und Nidhi für die tolle Einarbeitung in meine Experimente. Danke an Silke für die hilfreichen Lektionen im wissenschaftlichen Schreiben. Danke an Sophie, Marina, Alex und Patrick für den gemeinsamen Austausch über das Neu-im-Labor-Ankommen. Danke an Melanie, Nicola, Sara und Hakim, dass ihr bei Fragen immer ein offenes Ohr hattet.

Mein Dank gilt auch allen Mitarbeitern des Instituts für Mikrobiologie und Hygiene sowie Gisela für die Koordination mit dem DZIF und dem DZIF selbst für die finanzielle Unterstützung.

Abschließend danke ich meiner Familie, meinen Brüdern Leo und Vincent, meinen Freunden und Joschka für die unerschütterliche Unterstützung. Ohne die Unterstützung meiner Eltern Claudia und Matthias wäre mein Studium in dieser Form nicht möglich gewesen.